Nanoscale

Accepted Manuscript

This article can be cited before page numbers have been issued, to do this please use: V. Ow, Q. Lin, J. H. M. Wong, B. Sim, Y. L. Tan, Y. Leow, R. Goh and X. J. Loh, *Nanoscale*, 2025, DOI: 10.1039/D4NR03706E.

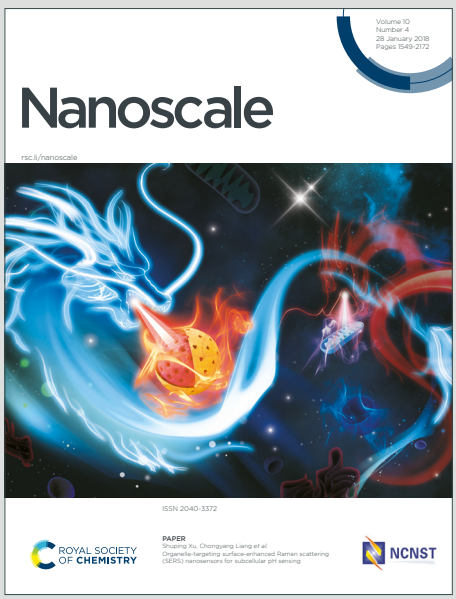

ROYAL SOCIETY OF CHEMISTRY

rsc.li/nanoscale

Understanding the interplay between pH and charges for theranostic nanomaterials

View Article Online
DOI: 10.1039/D4NR03706E

Valerie Ow[1,2], Qianyu Lin[1], Joey Hui Min Wong[1], Belynn Sim[1,3], Yee Lin Tan[1], Yihao Leow[1,3], Rubayn Goh[1,*], Xian Jun Loh[1,*]

[1] Institute of Materials Research and Engineering, Agency for Science, Technology and Research (A*STAR), Singapore
[2] Department of Biomedical Engineering, National University of Singapore (NUS), Singapore
[3] School of Materials Science and Engineering, Nanyang Technological University (NTU), Singapore

* For correspondence, please e-mail: R. Goh (rubayn_goh@imre.a-star.edu.sg), X. J. Loh (lohxj@imre.a-star.edu.sg)

Abstract

Nanotechnology has emerged as a highly promising platform for theranostic, offering dual capabilities in targeted imaging and therapy. Interactions between the nanomaterial and biological components determine the *in vivo* fate of these materials which makes the control of their surface properties of utmost importance. Nanoparticles with neutral or negative surface charge have a longer circulation time while positively charged nanoparticles have higher affinity to cells and better cellular uptake. This trade-off presents a key challenge in optimizing surface charge for theranostic applications. A sophisticated solution is an on-demand switch of surface charge, enabled by leveraging the distinct pH conditions at the target site. In this review, we explore the intricate relationship between pH and charge modulation, summarizing recent advances in pH-induced charge-switchable nanomaterials for theranostics over the past five years. Additionally, we discuss how these innovations enhance targeted drug delivery and imaging contrast, and provide perspectives on future directions for this transformative field.

View Article Online
DOI: 10.1039/D4NR03706E

1. Introduction

Coined by John Funkhouser in 2002, the term "theranostic" is a portmanteau of diagnostic and therapy (*1*). Prior to beginning treatment, it is crucial to perform diagnostic imaging to understand the cellular phenotype of the diseased tissue for therapeutic response assessment (*2*). Instead of developing separate materials for diagnosis and treatment, theranostic amalgate these modalities into one "package" (*3*). For clarity, this review defines theranostic materials as those which have combined imaging and therapeutic modalities in a single administration. By delivering imaging and therapeutic agents in the same dose, theranostic provides the ability to image and monitor the diseased tissue, delivery kinetics and drug efficacy *in vivo* and control the response to external stimuli such as heat and light in photothermal and photodynamic therapy (*2, 4*). Ultimately, theranostic aims to attain precise control of therapy and dose (*2*). The combination of diagnostics and therapeutics has opened the doors for precise diagnosis and personalized treatments in many diseases such as cancer (*5-7*), vascular diseases (*8-10*), cartilage diseases (*11-13*), kidney diseases (*14-16*), Alzheimer's disease (*17-19*) and bacterial infections (*20-22*).

Nanotheranostic is the combination of diagnostic and therapeutic modalities into a single delivery vector using nanotechnology (*23*). Nanocarriers are promising as they can localize and target the disease site and mitigate undesired side effects (*24*). Their unique intrinsic properties such as their nanosize make nanoparticles very attractive for localization in pathological lesions, especially in the case of cancer. Owing to the leaky vasculature and poor lymphatic drainage within the tumor microenvironment, nanocarriers can easily extravasate from the blood pool and preferentially accumulate in solid tumors in a phenomenon termed enhanced permeability and retention (EPR) (*25, 26*). Additionally, the high surface-area-to-volume ratio endow nanoparticles with high loading capacities of imaging probes and therapeutic drugs (*24*). Therefore, using nanomaterials in theranostic may be more effective in diagnosing and treating diseases at the cellular and molecular level due to its prolonged blood circulation, evasion of host defence mechanism and localization of theranostic agent at target site.(*27*)

Nanomaterials can be endowed with stimuli-responsiveness to better suit their theranostic purpose.(*28*) Smart nanotheranostic agents can be engineered to respond to intrinsic physicochemical and pathological factors in diseased regions such as pH and redox potential or external stimuli such as ultrasound, heat and light (*29*). In the presence of the stimulus, the nanocarrier can exhibit a range of responses such as a change in their hydrophobicity/hydrophilicity, degradability, charge and conformation which can in turn lead to ligand activation and controlled on-demand drug release (*29-31*). Amongst all stimuli, pH is one of the most powerful due to the distinct pH at various pathological sites *in vivo* which has led to pH targeting as a ubiquitous strategy in many theranostic applications. Recently, mesoporous silica nanospheres conjugated with an acidity-triggered rational membrane peptide demonstrated efficient targeting and cellular uptake in the acidic tumor microenvironment (*32*). This allowed the lanthanide-doped nanospheres to achieve magnetic resonance, thermal and fluorescence multimodal imaging while exhibiting near-infrared laser light-induced anticancer effects by combining photodynamic therapy and photothermal therapy *in vivo*.

pH-induced charge-switchable nanoparticles have garnered much attention because of their ability to adapt their surface charge in response to changes in their environment, allowing them to discern and target specific biological sites. Bernkop-Schnürch et al. recently published an excellent review on charge-reversible nanoparticles for theranostic where his team reviewed the different stimuli changes that can effect a charge reversal and how this can overcome biological barriers (*33*). Another notable review on charge-convertible nanoparticles is written by Lee et al. where his team reviewed the different pH-responsive functional groups that can reverse their charges such as the breakage of the acid-degradable benzoic imine bonds and the ionization of amine groups (*34*). pH-responsive groups can be protonated or deprotonated to give rise to a neutral, positively- or negatively-charged polymer (*30, 35*). This pH-dependent charge-switchable system can be tapped on to design nanocarriers that exploit the best of both worlds, reaping the benefits of both charges at appropriate periods *in vivo*. In this review, we first look at the main benefits of charged nanomaterials. We then discuss the different types of pH-responsive materials and their mechanisms. Next, we explore how certain factors such as

View Article Online
DOI: 10.1039/D4NR03706E

pH, salt and temperature can affect the physical properties of charged nanomaterials. Lastly, we review the recent advances in the field of theranostic using pH-responsive charge-switchable nanomaterials.

2. Benefits of charged nanomaterials

Charged nanomaterials offer significant advantages in pH responsiveness, biological interactions, and colloidal stability, making them highly promising candidates for theranostic applications. These properties can be leveraged to address key challenges in targeted drug delivery, enhanced imaging, and combined therapeutic and diagnostic strategies.

2.1. pH sensitivity

Mixed charge nanoparticles can exhibit pH-responsive behaviour when at least one of the charged components is a weak electrolyte as it can gain or lose charge due to the protonation or deprotonation with pH change (**Figure** 1A) (*36*). By carefully designing their formulation, the degree of ionization can be altered substantially to precisely tune their structure and properties at various pH (*37*). This pH-responsive reversible change in surface charge can be exploited to control interactions with biological molecules and cellular uptake. The various types of pH-responsive mechanisms will be discussed in Section 3.

2.2. Biological interactions

From proteins and nucleic acids to cellular membranes and bacterial walls, most biological molecules are charged. The building blocks of proteins are amino acids which contain ionizable carboxyl and amine groups. Approximately 10 % of protein structures have at least one charge cluster, mostly of mixed charge possessing equal cationic and anionic residues (*38*). Compared with proteins, nucleic acids are more negatively charged as its phosphate backbone has one negative charge per residue (*39*). While neutral phospholipids are mainly found in the outer leaflet of mammalian cellular membranes, most of the anionic phospholipids are located primarily in the inner leaflet; they carry negatively charged phosphate that link their hydrophilic headgroup to the lipid backbone (*40-42*). Similarly, both Gram-negative and Gram-positive bacteria have a net negative surface charge due to lipopolysaccharide and lipopolysaccharide, respectively (*43, 44*).

2.2.1. Cellular interactions and in vivo distribution

Due to the negatively charged cellular surfaces, positively charged nanoparticles exhibited stronger affinity to the cell membranes and higher rate of cellular uptake compared to neutral or negatively charged nanoparticles (**Figure** 1B) (*45, 46*). Their higher rate of cellular penetration may act as a double-edged sword as this may contribute to the higher cytotoxicity associated with positively charged nanoparticles (*47*). On the contrary, negatively charged nanoparticles have prolonged circulation time *in vivo* while their positively charged counterparts are cleared rapidly from the blood (*36, 48*). Neutral nanoparticles have the longest circulation time (*48*). Cho et al. reported the role of surface charge in cell adsorption and internalization using gold nanoparticles (*49*). It was observed that the cationic gold nanoparticles had 5-10 times higher cellular uptake efficiency than their neutral and negatively charged counterparts in 24 hours.

pH-sensitive charge conversion also provides an added advantage *in vivo*. Negatively charged or neutral nanoparticles can prolong circulation time and enhance tumor accumulation via the EPR effect (*50*). Upon reaching acidic regions, the nanoparticles undergo a charge conversion to positive,

View Article Online
DOI: 10.1039/D4NR03706E

promoting cellular uptake due to the negatively charged cell surface (*34*). For theranostics, this charge-switching behaviour enables pH-triggered drug release, targeted cellular uptake, and adaptive imaging contrast. In acidic tumor microenvironments or endosomal compartments, the shift in surface charge can enhance nanoparticle-cell interactions through charge-mediated endocytosis, promoting internalization. Additionally, pH-induced disassembly of micellar structures allows for site-specific release of encapsulated therapeutics, improving drug efficacy and minimizing off-target effects. From an imaging perspective, pH-responsiveness can be harnessed to improve the contrast of the nanoparticle in acidic tumor microenvironments or within cellular compartments (*51, 52*). The shift in charge can trigger aggregation, disassembly, or conformation changes in imaging agents, thereby amplifying their signal at the target site. This dual capability of site-specific imaging and triggered therapy highlights the potential of pH-responsive nanoparticles. Diagnostic, therapeutic and theranostic applications can leverage this pH-responsive charge switch which will be discussed in Section 5.

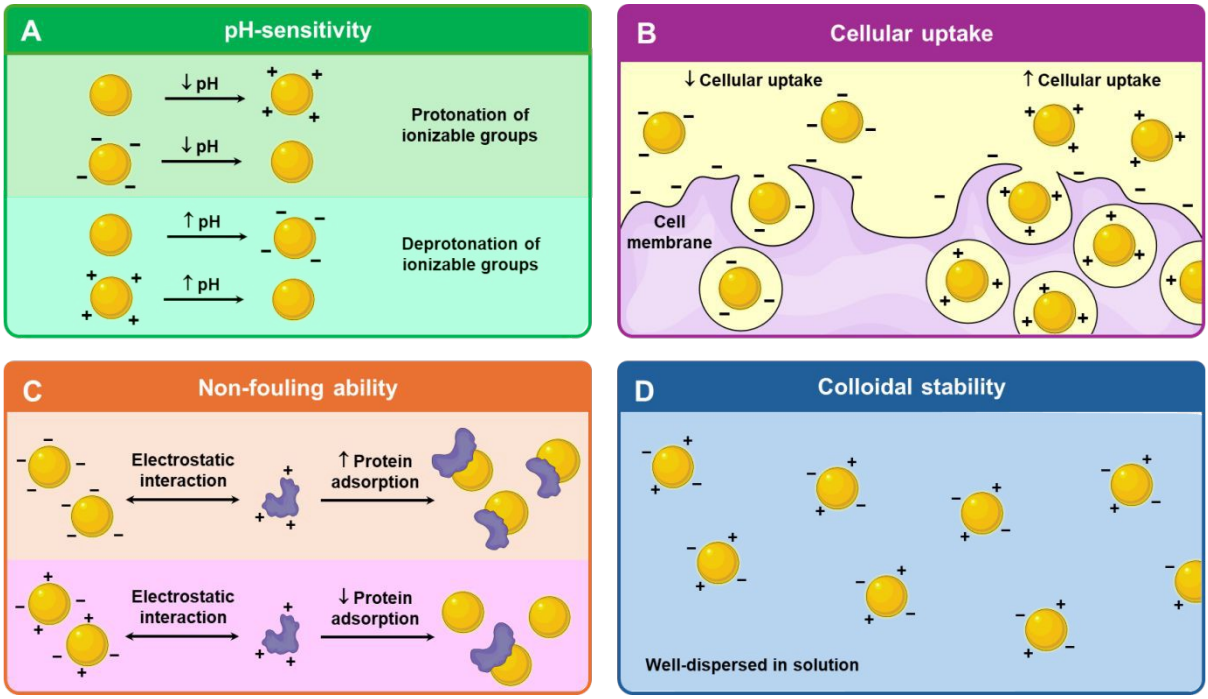

Figure 1. Benefits of charged nanomaterials. (A) Schematic of pH-sensitivity of charged nanoparticles. (B) Schematic of cellular uptake of negatively charged and positively charged nanoparticles. (C) Schematic of protein absorption of negatively charged and mixed-charge nanoparticles. (D) Schematic of a well-dispersed mixed charge nanoparticles in solution.

2.2.2. Protein adsorption and non-fouling ability

Non-fouling surfaces also known as "stealth" surfaces resist protein adsorption and cellular adhesion (*53*). Generally, surfaces that have strong protein adsorption will bind cells while surfaces that resist protein adsorption will resist cell adhesion (*53*). By electrostatic interactions, charged nanoparticles can have many undesirable non-specific interactions with biomolecules (**Figure** 1C) (*54*). For instance, non-specific protein interaction may facilitate particle opsonization which can lead to recognition by the mononuclear phagocytic system and fast clearance from the bloodstream before they can perform their intended application *in vivo* (*55, 56*). Li et al. demonstrated that the mixed charge gold nanoparticles modified with sulfonic negatively and positively charged ligand composition had better non-fouling ability compared to the single negatively charged ligand modified nanoparticles (*57*). The presence of both positive and negative surface charges creates a net-neutral surface potential that disrupts protein adsorption via a hydration layer near the surface as the heterogenous and mixed charges prevent stable electrostatic binding of proteins (*58*). By mitigating non-specific fouling, these charged

View Article Online
DOI: 10.1039/D4NR03706E

surfaces enhance the stability, stealth properties, and circulation time of theranostic systems, ultimately improving therapeutic delivery and imaging efficiency.

2.3. Colloidal stability

An important factor in determining the shelf life and feasibility of nanoparticles for *in vivo* applications is its colloidal stability (*36*). To reduce the high surface energy caused by their small size, nanoparticles tend to aggregate (*59*). According to the Derjaguin–Landau–Verwey–Overbeek (DLVO) theory, nanoparticles are characterized by an "electrical double layer" where electrostatic repulsive forces consistently counteract the attractive van der Waals forces to resist aggregation (*59*). To negate nanoparticle aggregation, a common approach is to design nanoparticles with surface charges to impart colloidal stability via electrostatic repulsion (*60*). Therefore, based on the DLVO theory, a greater net surface charge improves colloidal stability (*61*).

Additionally, mixed charge nanoparticles tend to have better colloidal stability compared to their singly charged counterparts. The presence of both positive and negative charges creates a heterogenous charge distribution that helps disrupt the formation of aggregation-prone particle-particle interfaces (**Figure** 1D). Unlike single-charge nanoparticles, which may experience attraction to oppositely charged species in the medium, the heterogeneous charge landscape in mixed charge nanoparticles prevents strong cohesive interactions, reducing particle-particle aggregation. This effect maintains a stable dispersion over time, enhancing colloidal stability. Ji's group which has been studying mixed charge nanoparticles extensively for over a decade, reported that the gold nanoparticles protected by mixed charge zwitterionic self-assembled monolayers enhanced stability compared to the singly negatively or positively charged gold nanoparticles (*62*). Moreover, the zwitterionic self-assembled monolayers exhibited long-term stability of the gold nanoparticles up to 6 months, ensuring longer shelf life, improved stability under physiological conditions, and sustained colloidal dispersion.

3. Types of pH-responsive mechanisms and their charge conversion

To attain the desired triggered release of theranostic payloads at specific pH levels, these nanoparticles are engineered with components that undergo a pH-induced switch in chemical composition or physicochemical properties (*63*), often tied to changes in surface charge or ionization states. pH-responsive materials fall into two main categories: those with acid-labile chemical bonds, which degrade at specific pH values, and those with ionizable chemical groups, which modulate surface charge in response to environmental pH (**Figure** 2) (*64*).

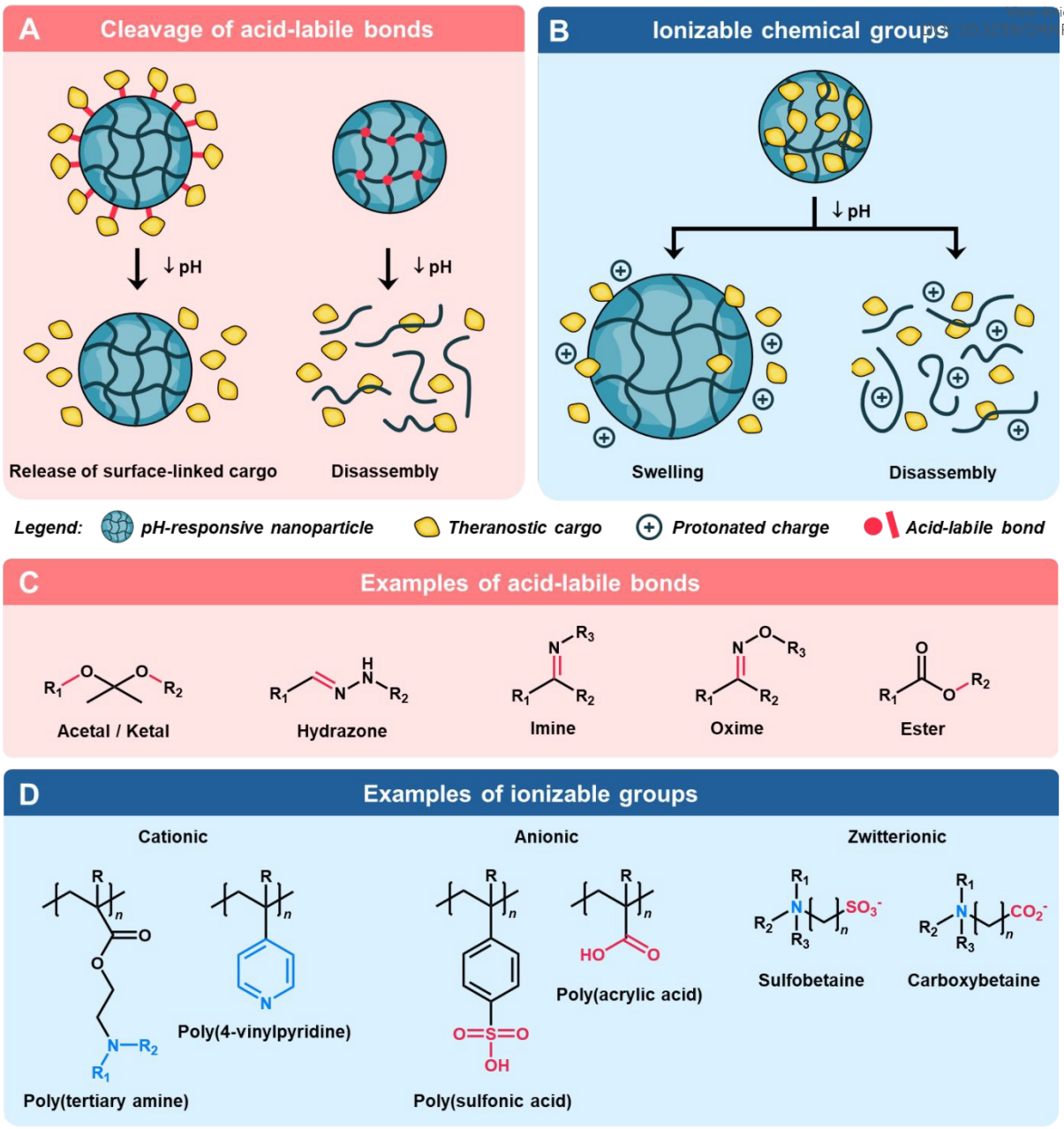

Figure 2. Overview of nanomaterial-based theranostic cargo delivery strategies using pH-triggered acid-labile bond cleavage and charge conversion. Schematic of (A) the mechanism of cargo release via cleavage of acid-labile bonds and (C) examples of such chemical bonds. Schematic of (B) the mechanism of cargo release via ionization of chemical groups and (D) examples of such groups.

3.1. pH-triggered acid-labile bond cleavage

The use of pH-induced cleavage of chemical bonds is a widely implemented strategy to achieve controlled delivery of theranostic agents (**Figure** 2A). This is commonly accomplished by employing acid-labile bonds, which serve either to covalently attach cargo molecules to the nanoparticle surface or act as crosslinkers, resulting in triggered disassembly of the nanoparticle (*64, 65*). Typical acid-labile bonds include imine, acetal/ketal, amide, ester/orthoester, and borate ester, which hydrolyze and degrade in the presence of an acidic environment (**Figure** 2C) (*66*). For instance, Palanikumar et. al. designed hybrid polylactic-co-glycolic acid (PLGA) core nanoparticles with a cross-linked bovine serum albumin shell that is functionalized with acidity-triggered rational membrane (ATRAM) peptides

View Article Online
DOI: 10.1039/D4NR03706E

(*67*). At pH 5.0, the acid degradation of the PLGA core due to the hydrolysis of the ester bonds led to a large increase in release rate of the encapsulated doxorubicin (DOX)-triphenylphosphine. It is worth noting that the cleavage of such pH-responsive bonds including β-carboxylic amide and benzoic imine can also lead to charge conversion by exposing ionizable moieties formed after acid hydrolysis (*68, 69*).

3.2. pH-triggered charge conversion via ionization

An alternative strategy involves incorporating ionizable functional groups onto nanoparticles, utilizing their selective protonation/deprotonation of moieties under varying pH conditions to achieve targeted delivery (**Figure** 2B). In contrast to systems containing acid-labile bonds, such charge conversion systems often exhibit a quicker response to pH changes, as the ionization process does not involve the breakage of strong chemical bonds (*70*). Through precise tailoring of the composition and proportions of functional groups, a diverse array of pH-responsive materials with charge conversion capabilities can be engineered. This versatile approach allows for the creation of cationic, anionic, and zwitterionic materials, each tailored to meet specific requirements in theranostic applications (**Figure** 2D).

3.2.1. pH-responsive positively charged materials

Cationic nanoparticles containing basic pendant groups such as piperazines and amino derivatives are one of the most widely used types of pH-responsive materials for theranostic applications (*71*). Below the pH threshold for these nanoparticles, protonation of the basic side chains is initiated, leading to a hydrophobic to hydrophilic conversion (*72*). This process also induces electrostatic repulsion between like-charged chains, prompting swelling or dissociation of the nanoparticle to release the encapsulant (*65*). Yan and coworkers developed a novel rodlike charge-conversion nanoparticle using amphiphilic dextran-b-poly(lactic-co-glycolic acid) (Dex-b-PLGA) and poly(2-(dimethylamino) ethylmethylacrylate)-b-poly(ε-caprolactone) (PDMAEMA-b-PCL) diblock copolymers (*73*). The nanoparticles were shown to exhibit reversible negative-to-positive charge transition at a slightly acidic pH, due to the ionization of amine groups on PDMAEMA, facilitating tumor cell uptake. This study presents a promising pH-responsive theranostic nanoplatform for targeted delivery of drugs or fluorescent agents to tumors.

3.2.2. pH-responsive negatively charged materials

Anionic materials contain acidic functional groups such as carboxylic acid and phosphoric acid to confer pH-responsiveness (*71*). Unlike cationic materials, anionic polymers in acidic conditions become protonated and hydrophobic, while they become deprotonated and hydrophilic in neutral or high pH environments (*72*). These materials are widely employed for the delivery of cationic cargo, such as DOX, facilitating the formation of stable complexes during blood circulation before the release of cargo at the intended site (*74*). Jia and coworkers fabricated a charge switchable nanoparticle based on poly(2-ethyl-2-oxazoline)-poly(methacryloyl sulfadimethoxine) (PEOz-b-PSD) and polyamidoamine/DOX (PAMAM/DOX) (*75*). At physiological pH, the stable nanostructure was formed by the electrostatic adsorption between the negatively charged PEOz-b-PSD shell and the positively charged PAMAM/DOX core. As the pH decreased to levels resembling the tumor microenvironment, protonation of PEOz-b-PSD led to the detachment of the surface shell polymers due to charge repulsion. This resulted in a substantial decrease in nanoparticle size from approximately 80

View Article Online
DOI: 10.1039/D4NR03706E

nm to less than 20 nm, exposing the positively charged ultrafine PAMAM/DOX core. This pH-induced charge transformation was found to significantly enhance the *in vivo* antitumor efficacy while reducing the cardiotoxicity of DOX.

3.2.3. pH-responsive zwitterionic materials

Zwitterionic nanoparticles, featuring both acidic pendant groups (anionic) and basic pendant groups (cationic), are extensively utilized as theranostic agents. In addition to their capability to swell in both acidic and basic environments, these amphoteric particles exhibit excellent stealth abilities during blood circulation (*76*). Their highly hydrated surface due to ionic solvation minimizes protein adsorption, contributing to prolonged circulation half-life, low cytotoxicity and enhanced therapeutic efficacy (*77, 78*). Moreover, by adjusting the relative ratios of acidic and basic moieties, nanoparticles can be tuned to exhibit charge conversion over a range of desired pH through isoelectric point modification (*70*). Wang and coworkers devised zwitterionic sulfobetaine functionalized polyacetal dendrimers as pH-responsive anticancer drug carriers (*79*). Through harnessing the synergistic charge reversibility of the sulfobetaine moieties and acid-labile cleavage of the acetal segments, the research team successfully achieved multi-level release regulation, demonstrating high cell internalization efficiency and cytotoxicity against cancer cells.

4. Factors affecting the physical properties of charged nanomaterials

The effective function of the charged nanomaterials is highly dependent on their size, solubility, and persistence in systemic circulation (*80*). As the charges on these nanomaterials are typically a result of ionizable groups, extrinsic factors such as pH, addition of salt and temperature strongly influence the physical properties of charged nanoparticles by tuning their inter-particle interactions. Herein, the influences of such factors on the physical properties of charged nanoparticles are summarized.

4.1. pH

pH is the main factor dictating the ionization of charged nanoparticles as most polyampholytes possess at least one protic ionizable component (*81*). Amongst ionizable functional groups, acidic electrolytes such as carboxylic and sulfonic acids and basic electrolytes such as ammonium and pyridine groups are commonly employed to imbue negative and positive charges on charged nanoparticles, respectively (*82*). These functional groups are pH-responsive by becoming protonated or deprotonated depending on pH fluctuations (*83*). It should be noted that pH sensitivity of charged nanoparticles is dependent on the strength of the electrolytes; nanoparticles with strong electrolytes such as trimethylammonium groups and sulfonic groups have muted pH sensitivity i.e., permanent positive and negative charges over the entire pH range (*84*). Hence, nanomaterials with mixed charge should possess at least one weak electrolyte ligand that can be ionized with pH change (*36*). For mixed-charged nanoparticles, a change in pH would alter the ratio of positive to negative charges and impact the overall electrostatic forces of attraction or repulsion which would subsequently determine nanoparticle dispersion or aggregation (*85*). This pH-dependent ionization can be tailored by determining its isoelectric point (IEP) which is defined as the pH where the polyampholyte is electrically neutral (*86*). As pH deviates from the IEP, electrostatic repulsion dominates and thus, mimicking polyanion or polycation behaviour and leading to solvation in aqueous solutions (*81*). Grzybowski and team showed

View Article Online
DOI: 10.1039/D4NR03706E

that mixed-charge nanoparticles have net positive charge and net negative charge at low and high pH, respectively (*87*). These like-charge repulsions at low and high pH stabilized the nanoparticle in aqueous solutions. However, when the surface charges on the mixed-charge nanoparticle is neutralized i.e., zeta potential is zero, precipitation will occur. This aggregation is attributed to the van der Waals attraction between nanoparticle cores and hydrogen bonding between the protonated groups (*87*). Generally, the polyampholyte is insoluble in aqueous solution at its IEP due to the dominant attractive forces (*81*).

By adjusting the ratio of positively and negatively charged ligands on the nanomaterial, Grzybowski's group who has long been working on mixed-charge gold nanoparticles, demonstrated that these nanoparticles can be designed to aggregate and precipitate within desired narrowed pH windows (*88*). Recently, the Grzybowski group reported a drug-free strategy to kill cancer cells by simply manipulating the aggregation state of the mixed-charge gold nanoparticles (*85*). These nanoparticles are well dispersed at physiological pH of 7.4 but aggregated into clusters of 50 – 100 nm in solid tumors (pH 6.5 – 6.9) and into supraparticles of 2 μm within cancer lysosomes of pH ≈ 4.8 thereby, disrupting the integrity of the lysosomal membrane and causing cell death. This pH-dependent aggregation is attributed to the protonation of acidic groups which led to an increased attraction due to van der Waals force and hydrogen bonding which outweighed the initial electrostatic repulsion that the dispersed nanoparticles experienced when they were negatively charged at high pH (*85*). Ji's group showed that a further reduction in pH would disperse the aggregated mixed-charged gold nanoparticles as the ammonium groups become increasingly protonated such that the electrostatic repulsion became more dominant than the attractive forces (**Figure** 3A) (*84*).

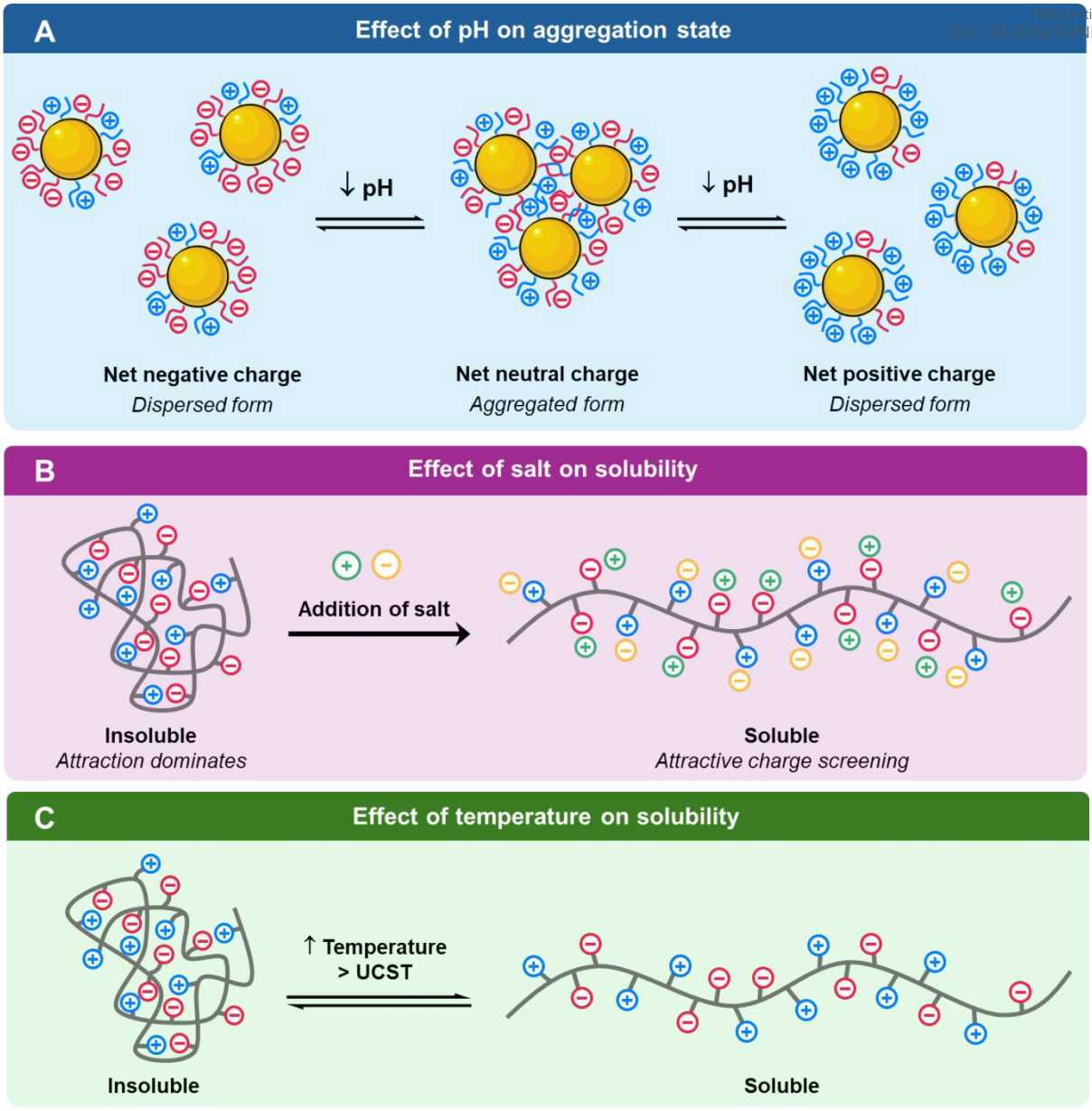

Figure 3. Schematic of (A) pH, (B) salt addition and (C) temperature on the physical properties of charged nanomaterials.

4.2. Salt

Besides pH, the stability of the charged nanoparticles in solution is highly responsive to the addition of salt especially for charged polymers. For singly charged polyelectrolytes such as polycations or polyanions, the addition of salt screens the charges and decreases inter- and intrachain repulsion of like charges (*81*). From an expanded or swollen form in pure water, the addition of salt would cause the polyelectrolyte to shrink (*89*). Beyond a critical amount of salt or critical ionic strength, the polyelectrolyte would precipitate out of solution as the inter- and intramolecular attractive forces become dominant. This phenomenon is known as the polyelectrolyte "salting out" effect. On the contrary, the addition of salt to polyampholytes screens their inter- and intrachain attraction and improves solubility compared to pure water (*81*). The polyampholyte chain expands in the presence of salt (**Figure** 3B) (*90*). This phenomenon is known as the antipolyelectrolyte "salting-in" effect. As

View Article Online
DOI: 10.1039/D4NR03706E

mentioned earlier, polyampholytes are insoluble and precipitate at their IEP but the addition of salt can help to effectively screen the attractive forces to aid solvation (*81*). Ji and colleagues reported that mixed charged gold nanoparticles could be stable in high salt solution of up to 2M NaCl whereas singly charged nanoparticles aggregated rapidly in the presence of salt (*62*). The high stability of the zwitterionic nanoparticles could be due to the hydration layer repulsion.

4.3. Temperature

Besides pH and ionic strength, temperature can also influence the size and solubility of the charged nanoparticles especially if they are formed from amphiphilic copolymers exhibiting either upper critical solution temperature (UCST) or lower critical solution temperature (LCST) behaviours (**Figure** 3C) (*90*). These critical solubility temperatures have been widely utilized for drug delivery with the polymers as drug carriers. Zwitterionic polymers generally exhibit UCST behaviour where they aggregate at lower temperatures and only solubilize upon warming (*91*). This is ascribed to the need to break the attractive electrostatic interactions in zwitterionic polymers. Generally, increased molecular weight is associated with higher UCST (*91*). Additionally, while the incorporation of polyanionic cosolutes lower the UCST, the presence of polycationic cosolutes increases the UCST (*92*). On the other hand, LCST is the opposite of UCST where polymers are well solvated at lower temperatures but rapidly aggregate upon warming. LCST can also be tuned by the polymer characteristics; high molecular weight and increased hydrophobicity are both associated with lowered LCST (*93*).

5. Tapping onto pH and charges of nanomaterials in imaging and therapy

To design nanomaterials for different theranostic applications, a key tool would be to exploit the distinct pH differences between the pathological tissues and healthy tissues. For example, the acidic tumor microenvironment can go to pH 5.6 (*94*), the gastric tract ranges from pH 1.0 – 2.0 in the stomach to pH 6.0 – 7.5 in the small and large intestines (*95*), atherosclerotic plaques are around pH 5.0 – 6.0 (*96*) and wounds can go to below pH 6.0 in acute wounds and pH 7.3 – 8.9 in chronic wounds (**Figure** 5A) (*97*). The pH-responsive segment of the nanomaterial should be engineered to charge-switch based on the pH at the target site. Next, the imaging and therapeutic cargo can be loaded into or on the nanoparticle (**Figure** 5B). A different pH environment can enhance the imaging contrast agents as seen from **Figure** 5C and will be discussed further in Section 5.1. Internal and external stimuli can result in therapeutic cargo release, sonodynamic therapy (SDT), photodynamic therapy (PDT) and photothermal therapy (PTT) (**Figure** 5D) which will be explored in Section 5.2. Lastly, exploiting the pH differences between pathological site and healthy tissues to induce a charge conversion from negative to positive allows for cellular uptake of the theranostic NP where it can exert its intended functions (**Figure** 5E).

View Article Online
DOI: 10.1039/D4NR03706E

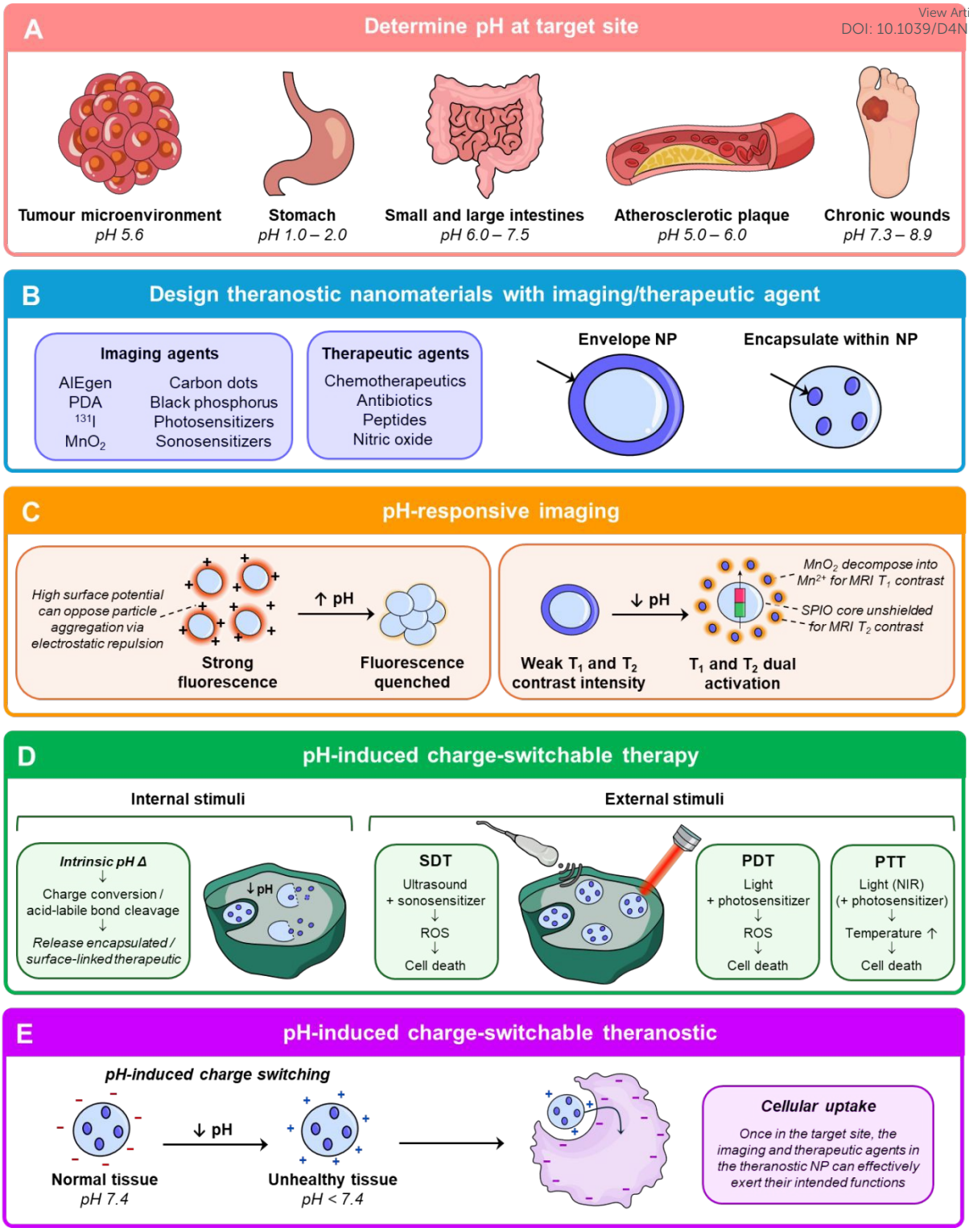

Figure 4. Schematic of designing pH-responsive charge-switchable theranostic nanomaterials. (A) Determine pH at the target site. (B) Design theranostic nanomaterials with imaging and/or therapeutic agent by either enveloping the nanoparticle (NP) or encapsulating within the NP. (C) Case studies of pH-responsive imaging. (D) pH-induced charge-switchable therapy via internal and external stimuli. (E) pH-induced charge-switchable theranostic which demonstrates how theranostic NP is taken up into target cell where it can exert its intended functions of imaging and therapy.

5.1. pH-responsive imaging applications

View Article Online
DOI: 10.1039/D4NR03706E

In vivo imaging techniques are important for early detection, diagnoses of diseases and precise monitoring of treatment. Nanomaterials are pushing the frontiers of imaging technologies by packing large payloads, yielding improved diagnostic sensitivity, multiplexing capacity, and modularity of design (*98*). The unique acidic or basic characteristics of different pathological sites *in vivo* enables the design of nanomaterials with a pH-responsive amplification of the emissive reporter signal at said sites (*80, 98*). Here, we review the various diagnostic modalities using pH-responsive nanomaterials.

5.1.1. Optical imaging

Optical imaging is an imaging technique widely used to investigate physical and biological systems based on the behavior of visible, ultraviolet, and infrared light (*4, 99*). It can be categorized as fluorescence imaging and bioluminescence imaging; both of which offer benefits such as high temporal resolution and sensitivity, non-invasive and relatively low cost (*4, 100*). Fluorescence imaging utilizes fluorophores that absorb the light energy (photon) of an external light source and emit light of lower energy and longer wavelength than the absorbed photon (*101*). This phenomenon is known as Stokes shift. Unlike fluorescence imaging, bioluminescence imaging utilizes native light emitted from a reaction between enzyme and substrate for monitoring and quantification of biological activity *in vivo* (*102*). However, optical imaging is limited by its signal diminution and shallow penetration depth caused by light scattering and absorption from surrounding tissues (*99*).

pH-responsive nanomaterials capable of differentiating tumors from surrounding healthy tissue have been developed to improve signal-to-noise ratio (*80*). A dual-responsive afterglow luminescent nanoprobe for peroxynitrite ($ONOO^-$) and pH was developed by Chen et al. (*103*). When exposed to $ONOO^-$ at physiological pH, the nanoprobes exhibits activated near-infrared (NIR) afterglow luminescence up to 14 days. By incorporating a twisted molecular geometry into the compound, aggregation-induced emission (AIE) can be achieved which enhanced its luminescent intensity and afterglow duration. Furthermore, the $ONOO^-$ -activated afterglow luminescence intensity decreases as pH drops which allows for the monitoring of acute skin inflammation development in three disease animal models (**Figure** 5A). This dual $ONOO^-$- and pH-responsiveness enabled the nanoprobes to precisely distinguish between allergies and inflammation in real time *in vivo* (**Figure** 5B).

View Article Online
DOI: 10.1039/D4NR03706E

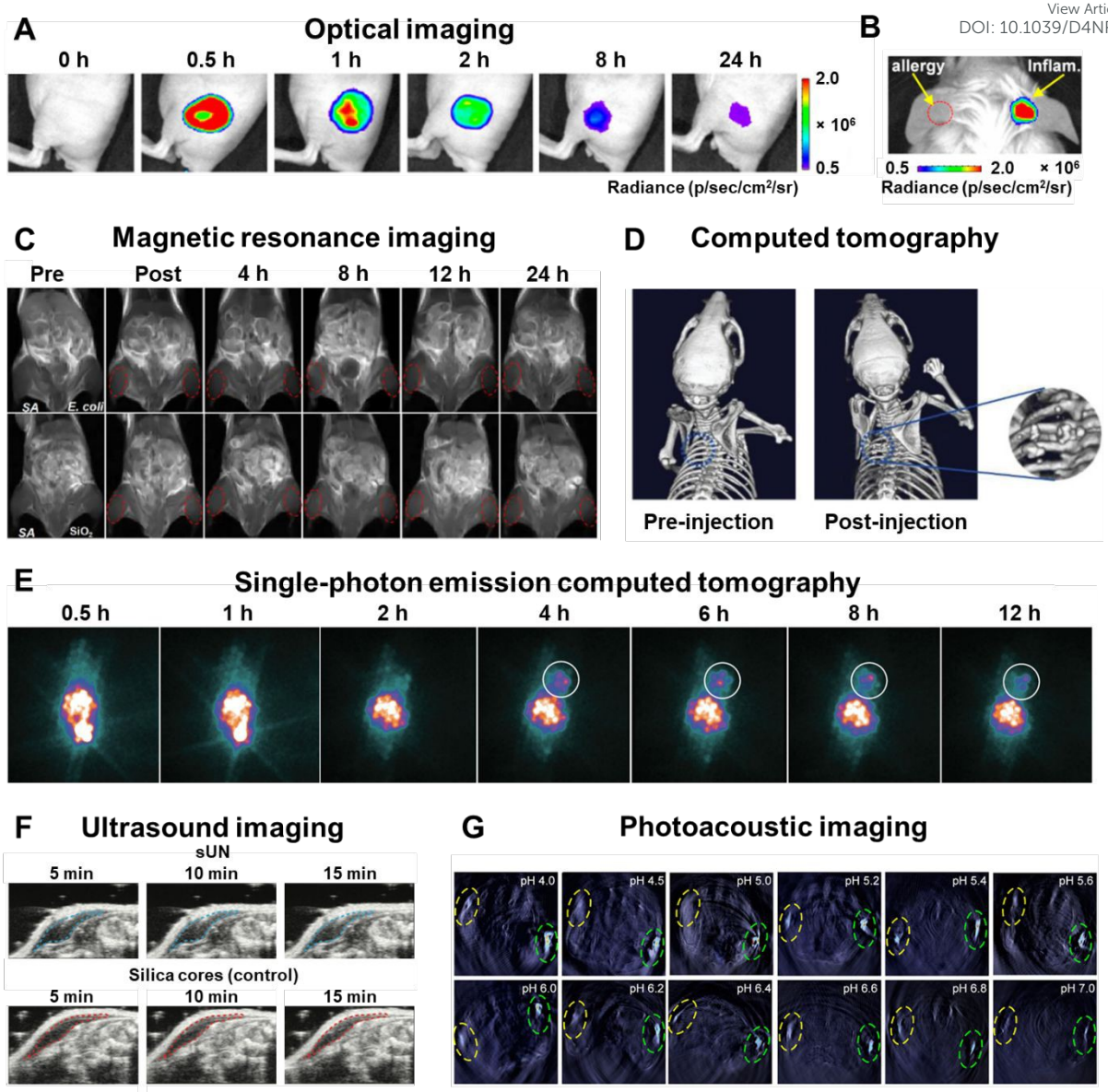

Figure 5. Diagnostic modalities using pH-responsive nanomaterials. (A) Afterglow images of the acute inflammatory lesions by *in situ* injection of preirradiated nanoprobes post lipopolysaccharide inoculation in mice. (B) Afterglow images of a mouse with allergic left ear and lipopolysaccharide-induced inflammatory right ear. The same amount of preirradiated nanoprobes were *in situ* injected into both the mouse ears, respectively, at 0.5 h post lipopolysaccharide inoculation. Adapted from Ref. (*103*). (C) T_1-weighted MR images of myositis at Pre, Post, 4, 8, 12, and 24 h after intravenous injection with the MRET probe. Adapted from Ref. (*104*). (D) Representative CT images of tumor-bearing mice treated with the NBOF-P-FA before and after 1 h of the injection. Adapted from Ref. (*105*). (E) SPECT images of C6 tumor-bearing mice at different time points post-injection the nanohybrid system. Adapted from Ref. (*106*). (F) Ultrasound imaging of sUN and silica cores control *in vivo* in mice models after 15 minutes post-injection of low-pH PBS to reduce local tissue pH. Adapted from Ref. (*107*). (G) Schematic diagram showing the injection method and the obtained PA images after the injection of PANI-BSA at different pH values (green ellipse: simulated tumor; yellow ellipse: control). Adapted from Ref. (*108*).

In another study, Ci et al. synthesized NIR-II fluorescent Fe-doped carbon dots with high quantum yield of 1.27 % and superior tissue penetration depth of approximately 6 mm (*109*). It displays a good linear relationship between fluorescence intensity and pH values with uniform fluorescence

View Article Online
DOI: 10.1039/D4NR03706E

intensity decline as pH changes from 2 to 6. The increased protonation of surface amine groups at acidic pH led to a high surface potential which can oppose particle aggregation via electrostatic repulsion. At higher pH, the surface zeta potential becomes less positive which leads to particle aggregation and quenching of their fluorescence. The NIR-II carbon dots also successfully realized real time *in vivo* tracking of gastric pH changes in three digestion processes in mice.

5.1.2. Magnetic resonance imaging (MRI)

Magnetic resonance imaging (MRI) relies on proton spin of endogenous water in the presence of an external magnetic field when excited with a radio frequency pulse (*110-112*). The excited protons quickly return to their initial state through relaxation when the pulse is turned off. Two independent relaxation parameters can be identified: longitudinal relaxation time (T_1) is the time required for longitudinal magnetization to recover to 63 % of its original magnitude and transverse relaxation time (T_2) is the time required for transverse magnetization to drop to 37 % of its initial magnitude (*113*). Tissues have unique proton density and water content which results in different T_1 and T_2 for image contrast to delineate anatomy and pathology (*111*). Although time-consuming and expensive, MRI can provide high spatial resolution, detailed three-dimensional anatomical information and high contrast between soft tissues (*4*).

Traditional contrast agents are modified to impart pH-responsive features to increase their selectivity for imaging specific microenvironments.(*114*) Lu et al. synthesized a pH-sensitive MRI contrast agent (SPIO@SiO_2@MnO_2) that displays low T_1 and T_2 contrast intensity under normal physiological conditions (*115*). However, the signals are restored under acidic microenvironments driven by MnO_2 layers being reduced to magnetically active Mn^{2+}. The degree of contrast quenching-activation can be modulated via the intermediate layer thickness of SiO_2 between SPIO and MnO_2. Obtained images showed a high contrast sensitivity between diseased and normal tissues. When deployed *in vivo*, it was capable of tracking liver metastases and tissue inflammation.

In another report published by Li et al., a pH-responsive magnetic resonance tuning (MRET) probe was fabricated for *in situ* MRI of bacterial infection *in vivo* (*104*). The enhanced T_1-weighted signal at the bacteria-infected acidic zone is attributed to the disassembly of MRET probe and conversion of T_2 contrast agent to T_1 contrast agent. Additionally, the MRET probes can bind specifically to cell walls of *Staphylococcus aureus* which led to the brightening of S. aureus-infected site compared to the negligible change in T_1 signal intensity at E. coli or sterile inflammation sites (**Figure** 5C). Therefore, the MRET probe can precisely diagnose and distinguish S. aureus infections from sterile inflammation or normal tissues which remain dark under T_1 imaging.

5.1.3. Computed tomography (CT)

Computed tomography (CT) leverages the detection of varying X-ray absorption density across different tissues as they pass through the body (*116*). This non-invasive imaging technique offers fast examination speed and high spatial resolution (*117, 118*). Nevertheless, contrast agents used for CT are limited and subjects are exposed to great amounts of radiation with unknown effects (*4*).

Nanomaterials as contrast agents can offer enhanced contrast and targeted imaging. For instance, Zhang et al. prepared a bismuth-based mesoporous nanoball (NBOF-P-FA) with surface modification of polyethylene glycol and folic acid conjugates which has contrast-enhanced CT imaging

View Article Online
DOI: 10.1039/D4NR03706E

capability (*105*). The EPR effect and folic acid-mediated targeting facilitated accumulation of the nanomaterial in the tumors of mice models which resulted in bright spots in the tumor on the CT image (**Figure** 5D).

5.1.4. Single-photon emission computed tomography (SPECT)

Single-photon emission computed tomography (SPECT) is a nuclear imaging technique that relies on the detection of emitted gamma rays from radionuclides during their radioactive decay (*119*). Collimators are used to accurately determine the origin of gamma ray photons (*120*). Coupled with high tissue penetration limit and high-sensitivity, SPECT can multiplex for simultaneous detection of multiple different targets (*98, 121*). However, SPECT also comes with its disadvantages such as high cost and radioactive exposure (*119, 121*).

Developed with pH-charge conversion property, an iodine-131 (^{131}I)-labelled polyethyleneimine (PEI)/DOX complex can enhance SPECT imaging of cancer cells (*106*). Alkoxyphenyl acylsulfonamide (APAS) was conjugated with PEI to induce surface charge conversion from neutral charge at physiological pH to positive charge at acidic pH, which enhanced the cellular uptake by cancer cells and in turn improved SPECT imaging *in vivo* (**Figure** 5E).

5.1.5. Ultrasound (US) imaging

In ultrasound imaging, high frequency sound waves reflect off tissues and images are constructed via the pulse-echo principle (*98, 122*). Ultrasound imaging is low cost, non-invasive and has high tissue penetration ability with little side effects on surrounding tissues (*123*). However, it has low contrast due to negligible differences in composition, density and echogenic properties of various tissues (*124*).

To improve ultrasound contrast and signal stability, Walker et al. developed a solid ultrasound nanosensor (sUN) with a pH-responsive poly(methacrylic acid) (PMA_{SH}) layer separating the silica core and shell (*107*). At physiological conditions, the PMA_{SH} layer expands due to repulsion from the deprotonated acid groups. These acid groups become protonated at low pH which causes contraction of the PMA_{SH} film against the silica core. Two clear silica interfaces for scattering/reflection are formed which enhances the ultrasound signals (**Figure** 5F). Moreover, the pH-dependent stiffness and subsequent density change of the PMA_{SH} layer contributed to the ultrasound enhancement in acidic conditions. The prepared sUN demonstrated a 2-fold ultrasound contrast increase in response to a shift in pH from pH 7 to 6 and 6 to 5.

5.1.6. Photoacoustic (PA) imaging

Photoacoustic (PA) imaging is a hybrid bioimaging modality that combines optical excitation with ultrasonic detection (*125*). Biological tissues absorb energy from non-ionized laser pulses and convert it into heat thereby generating ultrasonic waves due to transient thermoelastic expansion (*126*). While fluorescence imaging has shallow penetration depth, PA imaging allows for deeper tissue penetration and higher spatial resolution due to the ultrasound modalities (*125*). pH-sensitive nanomaterials can enhance the signal-to-noise ratio by amplifying PA signal only at specific pH regions while maintaining a dormant state in normal tissues (*80*).

View Article Online
DOI: 10.1039/D4NR03706E

Yang et al. devised a pH-responsive polyaniline-bovine serum albumin (PANI-BSA) probe for accurate pH detection in tumors via PA (*108*). A linear correlation between PA signal and pH within the range of 5 – 6.8 was demonstrated *in vitro* and *in vivo* (**Figure** 5G). The pH of separate tumor types can be differentiated owing to its superb anti-interference ability. Moreover, the highly pH-sensitive probe can produce high-resolution images and is deemed safe for *in vivo* PA imaging in mice models.

5.2. pH-induced charge-switchable nanomaterials for therapeutic applications

5.2.1. Internal stimuli

Due to the distinct pH differences between pathological and healthy tissues, pH is one of the most applied stimuli for charge conversion. Designing pH-responsive nanomaterials which can alter their surface charge, takes advantage of the intrinsic pH conditions *in vivo* to effect a therapeutic action such as drug release at the target site.

The widespread misuse of antibiotics has fuelled the rise of multidrug-resistant bacterial strains, which diminishes the effectiveness of antibiotic therapies for bacterial infections (*127*). This resistance is further exacerbated by the formation of biofilms where bacteria aggregate within a protective matrix of extracellular polymeric substances and prevent penetration of antibacterial agents (*128*) While cationic nanomaterials can penetrate biofilms, their treatment efficacy is limited by poor circulation ability (*128*). To address this challenge, pH-induced charge-switchable nanomaterials leverage acidic bacterial infection sites to undergo charge reversal thus, transforming into positively charged particles that specifically bind onto negatively charged cell walls of pathogens. For the treatment of Methicillin-resistant *Staphylococcus aureus* (MRSA) infection, Li and colleagues designed a pH-responsive nanosystem based on poly(β-amino esters)-methoxy poly(ethylene glycol) to encapsulate linezolid, the first approved oxazolidinone antibiotic (*129*). The cationic nanocarrier was neutralized with the addition of low molecular weight hyaluronic acid (HA) to mask its positive charges in physiological conditions for an extended circulation time. Upon reaching the acidic biofilm microenvironment, the poly(β-amino ester) groups are protonated while the HA shell is degraded by hyaluronidase present in bacteria. Collectively, this negative to positive surface charge conversion promoted bacterial binding and biofilm penetration thereby accelerating linezolid release. This nanosystem eliminated almost all MRSA cells in an abscess-bearing mice model after five days of treatment. Similarly, other studies have also utilized pH-responsive charge reversal to release and nitric oxide (*130*) and cinnamaldehyde (*131*) for efficient *in vivo* antibacterial results via bacterial membrane disruption, cell apoptosis and macrophage activation.

Similarly, in oncology, the acidic tumour microenvironment presents an opportunity to be strategically exploited for tumour-targeted therapy. Rapidly metabolising tumours lead to an overproduction of lactic acid and decrease in extracellular pH which makes pH-responsive charge switchable nanosystems attractive for site-specific therapy (*33*). Several nanoplatforms have taken advantage of the pH-triggered negative to positive surface charge reversal to achieve deep tumour penetration and intracellular uptake of anticancer drugs. This is done through pH-responsive mechanisms such as the breakage of acid-labile linker between polymer and drug, cleavage of the amide bond to expose the cationic amino groups (*132*), protonation of pyrrole ring (*133*) and protonation of acylsulfonamide groups (*134*) which have resulted in effective drug delivery for cancer therapy in mice tumor models. Notably, Yang et al. reported a three-pronged synergistic cancer treatment using an NGR-poly(ethylene glycol)-poly($_L$-lysine)-dimethylmaleic anhydride polymer loaded with abemaciclib and IMD-0354 (*135*). Due to the hydrolysis of acid-labile amide bonds in dimethylmaleic anhydride (DMMA), the negative to positive surface charge conversion and reduction in size improved cellular uptake and cargo release. Apart from the chemotherapeutic effects of abemaciclib and IMD-0354, the former inhibited regulatory T cell proliferation while the latter enhanced tumour-associated macrophage repolarization which together caused a significant inhibition of tumour growth *in vivo*.

Aside from bacterial infection and cancer, pH-induced charge switchable nanosystem has found an avenue in Alzheimer's disease (AD). By targeting the fibroblast growth factor receptor 1 (FGFR1)

View Article Online
DOI: 10.1039/D4NR03706E

overexpression in the blood−brain barrier and cholinergic neuron, Qian et al. functionalized FGFR1-ligand (FGL) onto citraconylation-modified poly(ethylene glycol)-poly(trimethylene carbonate) nanoparticles loaded with hybrid peptide HNSS (*136*). The resultant FGL-NP(Cit)/HNSS nanosystem could target the cholinergic neurons in lesion site through FGFR1-mediated endocytosis. Due to the hydrolysis of the ß-carboxylic amide bond in the acidic lysosomal microenvironment, the nanosystem underwent a negative to positive charge conversion which facilitated lysosomal escape (**Figure** 6A). Furthermore, this charge conversion weakened the electrostatic interaction between HNSS and FGL-NP(Cit), which in turn enlarged particle size and enhanced HNSS release (**Figure** 6B). The FGL-NP(Cit)/HNSS treatment group exhibited the best restoration of spatial cognition and memory in a Morris water maze test with escape latency comparable to the normal control wild type (WT) mice (**Figure** 6C).

View Article Online
DOI: 10.1039/D4NR03706E

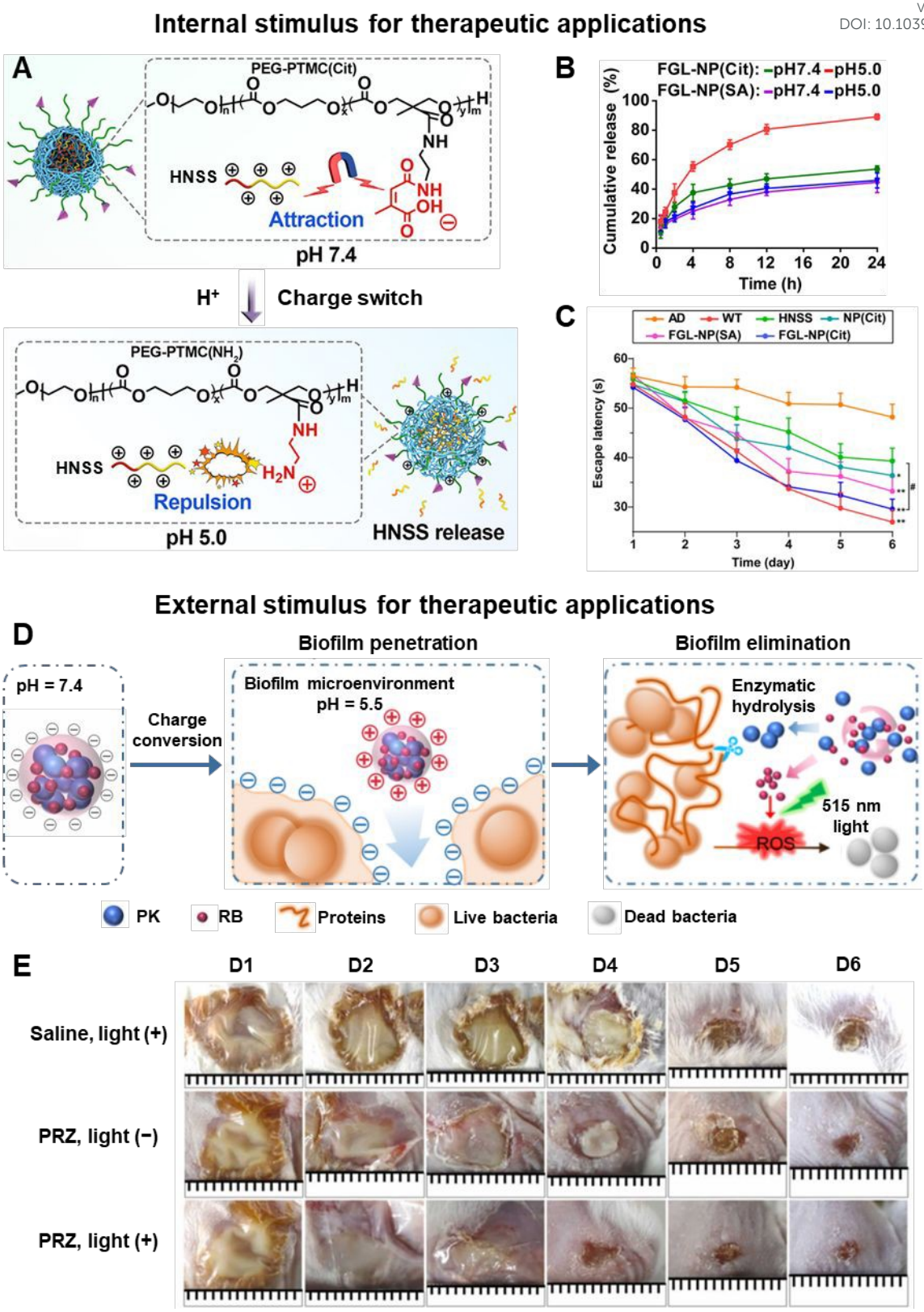

Figure 6. Therapeutic applications using pH-responsive charge-switchable nanomaterials. (A) Schematic of the acid-triggered charge reversal and release of HNSS from FGL-NP(Cit)/HNSS. (B) *In vitro* release profile of HNSS from FGL-NP(Cit) and FGL-NP(SA) (no charge-switching feature). (C) Mean escape latency in the Morris water maze experiment of the treated mice. Adapted from Ref. (*136*). (D) Schematic of the charge conversion of PRZ nanoparticle in acidic biofilms and visible light irradiation. (E) Photographs of wound infection in mice with saline and PRZ injected on day 1, 2 and 3. Adapted from Ref. (*137*).

View Article Online
DOI: 10.1039/D4NR03706E

5.2.2. External stimuli

Apart from endogenous stimuli, exogenous stimuli such as light (phototherapy) or ultrasound (sonotherapy) have also been widely explored to evoke a therapeutic effect non-invasively (*138-141*). Phototherapies such as photodynamic therapy (PDT) and photothermal therapy (PTT) harness light of various wavelengths to generate cytotoxic reactive oxygen species (ROS) and increase temperature, respectively within a target tissue (*138*). For instance, Ding and co-workers loaded proteinase K (PK) and photosensitizer Rose Bengal (RB) into a zeolitic imidazolate framework-8 (ZIF-8) for enzymatic hydrolysis and PDT against biofilm infections (*137*). The resultant pH-responsive nanocomplex (PRZ) was negatively charged at physiological conditions but became positively charged in the acidic biofilm due to the acid-sensitive decomposition of ZIF-8 (**Figure** 6D). This charge switch enhanced the PRZ penetration into the negatively charged biofilm and accelerated release of PK and RB. PK will hydrolyze the biofilm matrix protein while RB, under visible light irradiation, will generate ROS to eradicate bacteria in the biofilm. The synergistic biofilm elimination of PRZ accelerated the wound healing process in a mice wound infection model (**Figure** 6E).

In PTT, light (typically within the near-infrared region) can raise the tissue temperature for local photocoagulation, thereby inducing rapid cell death via protein denaturation and cell membrane damage (*138*). Prolonged hyperthermia under strong laser intensity will cause excess heat diffusion and undesirable inflammation to surrounding healthy tissues. To this end, Ma et al. integrated PTT with nitric oxide (NO) release from pH-responsive charge reversible nanosystem to enhance anti-biofilm treatment (*142*). This PDG@Au-NO/PBAM nanosystem was composed of thermo-sensitive NO-donor conjugated gold nanoparticles on cationic poly(dopamine-co-glucosamine) as the core and anionic phenylboronic acid-acryloylmorpholine copolymer as the shell. In the acidic biofilm, the polymer shell was degraded via cleavage of the boronate ester bond between the shell and core which in turn exposed the cationic core. The positively charged surface enhanced the infiltration and accumulation of PDG@Au-NO/PBAM in the biofilm. Upon NIR irradiation, PDG@Au-NO/PBAM generated high doses of NO to effectively eradicate biofilm. The PDG@Au-NO/PBAM was unable to eradicate methicillin-resistant *Staphylococcus aureus* (MRSA) and *Escherichia coli* (TREC) biofilm without near-infrared irradiation but achieved more than 99% bacteria killing under NIR irradiation of 808 nm at 1.0 W/m^2 for 10 minutes. Thus, this shows that integration of photothermal therapy with pH-responsive charge reversible nanosystem can lead to a more effective biofilm eradication.

5.3. pH-induced charge-switchable nanomaterials for theranostic applications

By combining both diagnostic and therapeutic modalities, pH-induced charge switchable nanomaterials can represent a pivotal innovation with profound influence in theranostic applications, particularly in combating infections and treating cancer. The recent developments in the past five years (2020 – 2024) of such pH-induced charge switchable nanomaterials for theranostic purposes with real time *in vivo* monitoring are summarized in Table 1.

With the ability to be precisely imaged, these theranostic nanomaterials are useful to improve therapeutic efficacy in treating multi-drug resistant bacterial infections without antibiotics while also addressing the issue of microbial drug resistance. Ji and team engineered pH-sensitive nanocarriers (α-CD-Ce6-NO-DA) to deliver nitric oxide (NO) and chlorin e6 (Ce6) for effective eradication of MRSA biofilm via PDT (*128*). Surface charge of the nanocarriers changed from negative at pH 7.4 to positive at acidic biofilm of pH 5.5 facilitated excellent biofilm penetration and retention as verified by the strong fluorescence at infection site 24 hours post-injection. This mechanism stems from the hydrolysis of amide bonds of the copolymer in acidic conditions owing to the strong electron-pulling effects of carboxyl groups. The rapid NO release in response to overexpressed glutathione (GSH) in the biofilm kills bacteria, reduces GSH levels and generates reactive nitrogen species which further bolsters PDT efficiency. The NO synergistic PDT of α-CD-Ce6-NO-DA significantly improved bactericidal effect and wound healing speeds in MRSA-infected mice models.

View Article Online
DOI: 10.1039/D4NR03706E

Recently, Kong et al. developed pH-switchable nanoparticles denoted as GPBO to treat bacterial infection in diabetic wound models via photothermal-catalytic therapy (*143*). GPBO were synthesised by functionalising bismuth oxyiodide ($BiO_{1-x}I$) core with polydopamine (PDA) and glycol chitosan (GCS). GPBO demonstrated conversion of surface charge from negative under physiological pH to positive in acidic infection sites of pH 6.5 (**Figure** 7A). The free amine groups of GCS acquired positive charges when pH drops below their pKa of 6.5. Consequently, strong electrostatic interactions between positively charged GPBO and negatively charged bacterial cell wall facilitated GPBO accumulation at the wound site. Conversely, the negative charge of GPBO at physiological pH ensures minimal affinity to negatively charged normal cells, thereby enabling selective eradication of pathogens while safeguarding normal neighbouring cells. In mouse subcutaneous abscess models, GPBO showcased excellent photothermal and CT imaging capabilities (**Figure** 7B). Upon NIR irradiation, GPBO promoted the healing of diabetic wound models with antibacterial and anti-inflammatory effects (**Figure** 7C).

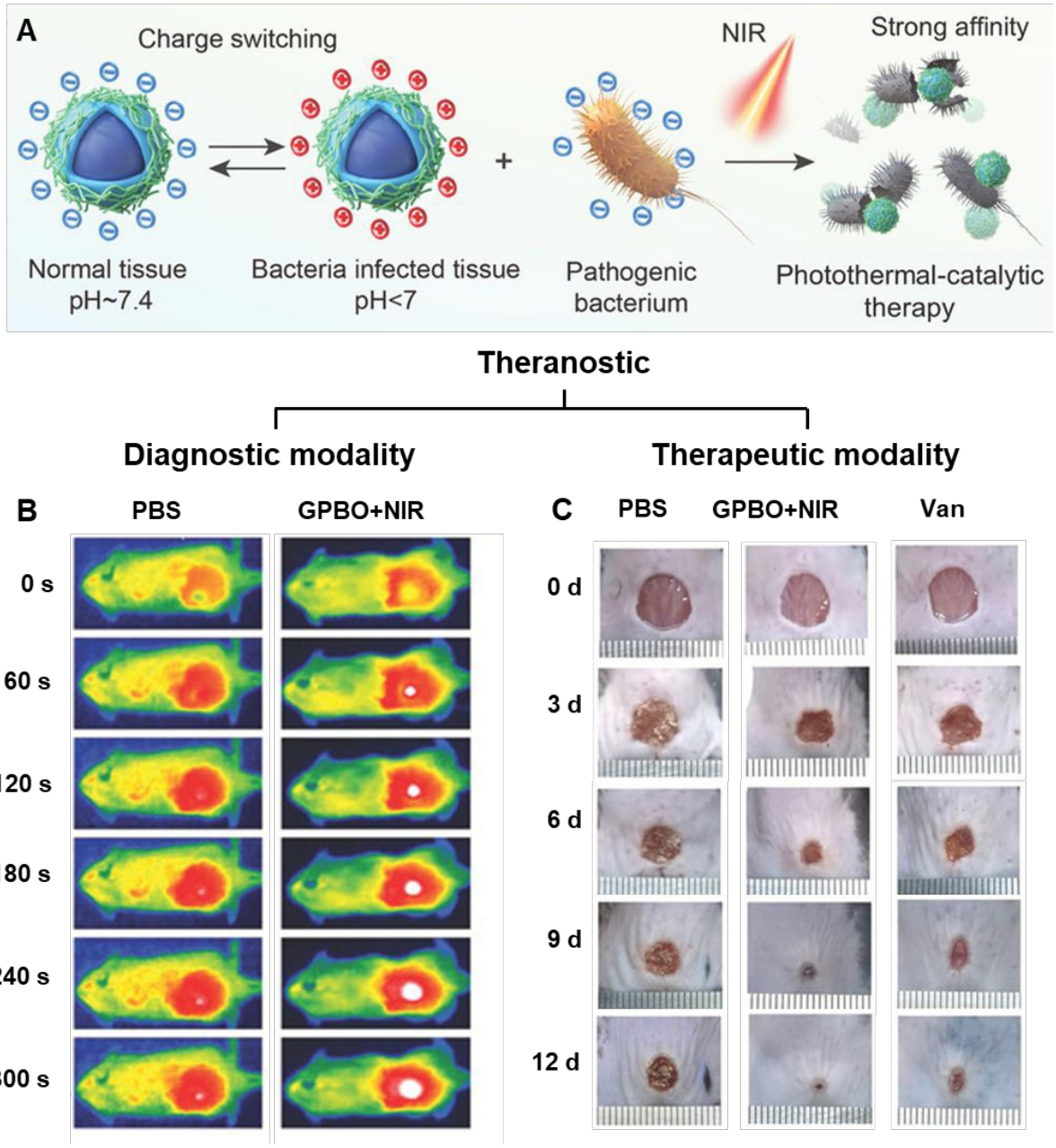

Figure 7. Theranostic applications using pH-responsive charge-switchable nanomaterials. (A) Schematic of the mechanism of pH-responsive surface charge switch of GBPO nanoparticles from negative to positive in the acidic environment of bacterial infection site. GPBO aggregate at the wound due to the negatively charged bacterial cell

View Article Online
DOI: 10.1039/D4NR03706E

wall to achieve a targeted antibacterial therapy, which could be further enhanced with NIR irradiation because of the photothermal-catalytic properties of GPBO. (B) Real-time infrared images of the cyst site of the subcutaneous abscess mouse model at 12 h after the intravenous injections of PBS and GPBO NPs. (C) Photographs of the diabetic wound area at different time points of the treatment groups. Vancomycin (Van) is used as the positive control. Adapted from Ref. (*143*).

Leveraging the pH-sensitive nature of GCS to realize charge conversion in acidic environment, Yan and co-workers also utilised GCS to functionalise polyaniline-grafted persistent luminescence NPs (PLNP) termed PLNP@PANI-GCS for precise PTT guided by persistent luminescence imaging (*144*). Similar to the abovementioned GPBO, PLNP@PANI-GCS becomes positively charged in acidic bacterial-infection abscesses and forms electrostatic interactions with negatively charged bacteria *in vivo*. This cluster of nanoparticles at the infection site offered enhanced photothermal effects compared to neighbouring regions which led to the spatial precision of NIR irradiation and targeted heating directly to bacteria. *In vivo* imaging-guided PTT of bacterial-infection abscesses demonstrated successful treatment, with over 99% eradication of three bacterial strains (*E. coli*, *S. aureus*, and MRSA).

Moving to the field of oncology, Whittaker and his group designed pH-responsive ZIF-8 nanoparticles functionalised with low-fouling fluoropolymers (PFSAM) for image-guided tumour therapy (*145*). This nanoplatform enables sensitive *in vivo* monitoring via ^{19}F MRI and extended circulation time in the bloodstream due to its hydrophilic and low-fouling corona. The acidic tumor microenvironment triggered the gradual degradation of ZIF-8-PFSAM nanoparticles and release of zinc ions and encapsulated DOX. Apart from triggering cancer cell apoptosis, the dissociated zinc ions also coordinate with sulfoxide moieties in the fluoropolymers to cause hydrophilic to hydrophobic switch and negative to positive surface charge conversion. This transition diminishes their stealth-like nature and promotes specific uptake by cancer cells within the tumour. ZIF-8-PFSAM treatment completely stopped tumor growth after 12 days post-injection and improved survival rates in mice.

Another MRI-guided cancer therapy was reported using a multifunctional synergistic nanoplatform which comprised of catalase and manganese dioxide (MnO_2) encapsulated into Ce6-modified GCS polymeric micelles (*146*). GCS undergoes neutral to positive charge conversion in the acidic tumor microenvironment thereby promoting accumulation of Ce6 within the tumor. Furthermore, catalase aids in reoxygenating the hypoxic tumour tissues while MnO_2 reduces intracellular GSH and generates Mn^{2+} as a contrast agent for T_1-weighted MRI. The nanoplatform enhanced the efficacy of PDT against HeLa tumours and improved survival rates after 10 weeks in mice.

Apart from charge switch, pH was employed to induce a size switch in multifunctional nanomicelles (PCR7780-APP) fabricated with anti-programmed death ligand 1 peptide inhibitor (APP) in its core to preserve its bioactivity (*147*). These nanomicelles (~ 121.1 nm, 2.3 mV) were of optimal size for the EPR effect but upon reaching the acidic tumor microenvironment, promptly switched to smaller unimolecular micelles (~ 24.1 nm, 19.6 mV) for deeper tumor penetration and accumulation. The released APP and ultrasound-induced ROS from CR780 augmenting immune T-cell recruitment and activation in deep tumor tissues thereby achieving effective sono-immunotherapy under precise fluorescence and PA imaging.

Table 1. *In vivo* theranostic applications of pH-induced charge-switchable nanomaterials in the last five years (2020 – 2024).

Disease	**pH-responsive mechanism**	**pH change**	**Charge conversion**	**Imaging modality (imaging agent)**	**Therapeutic modality**	**Ref.**
Bacterial infection	Hydrolysis of amide bond in PEG block polypeptide copolymer	pH 7.4 to 5.5	−16 to +7.5 mV	Fluorescence imaging (Ce6)	NO release and PDT under 660 nm laser	(*128*)

Bacterial infection in diabetic wounds	Protonation of amine groups in GCS (pKa ≈ 6.5)	pH 7.4 to 6.5	−7.9 to +19.5 mV	Photothermal imaging (PDA), CT ($BiO_{1-x}I$)	PTT under 808 nm NIR laser irradiation	(*143*)
Bacterial infection	Protonation of amine groups in GCS	pH 7.4 to 6.5	−4.7 to +19.0 mV	Persistent luminescence imaging (PLNP)	PTT under 808 nm NIR laser irradiation	(*144*)
Ocular bacterial infection	Hydrolysis of β-carboxylic amide	pH 7.4 to 5.5	−29 to +28 mV	Fluorescence imaging (phenothiazinium dye)	PTT under 650 nm laser irradiation	(*148*)
Cancer	Degradation of ZIF-8 from breakage of bond between zinc ions and 2-methylimidazole (MIM)	pH 7.4 to 6.5	−4 to +4 mV	^{19}F MRI (PFSAM)	DOX and zinc ions release	(*145*)
Cancer	Protonation of amine groups in GCS	pH 7.4 to 6.5	−0.1 to +7.4 mV	T_1-weighted MRI (MnO_2)	PDT under 660 nm laser irradiation	(*146*)
Cancer	Protonation of carboxyl and amine groups (pKa of CR780≈ 6.73)	pH 7.4 to 6.5	+2.3 to +19.6 mV	Fluorescence, PA imaging (CR780)	SDT with APP release	(*147*)
Oral cancer	Hydrolysis of DMMA, protonation of amino groups of PAH	pH 7.4 to 6.5	−14.32 to +16.35 mV	Infrared thermal imaging (black phosphorus, PDA)	PTT under 808 nm NIR laser irradiation	(*149*)
Cancer	Cleavage of amide bond in DMMA	pH 7.4 to 6.5	−21.6 to +4.0 mV	Fluorescence imaging (Ce6)	PDT under 660 nm NIR laser irradiation	(*150*)
Cancer	Protonation of sulfamine group in alkoxyphenyl acylsulfonamide (APAS)	pH 7.5 to 6.0	−2.5 to ≈ +16 mV	SPECT, CT (^{131}I)	Radiotherapy	(*151*)
Cancer	Protonation of sulfamine group in APAS	pH 7.5 to 5.0	≈ −3 to +16.5 mV	SPECT (^{131}I)	DOX release and radiotherapy	(*106*)

6. Conclusion and perspectives

In this review, we discussed the benefits of charged nanomaterials such as their favourable biological interactions, colloidal stability and pH sensitivity. We then looked deeper into pH-responsive mechanisms through acid-labile bond cleavages or charge conversion. Next, we explored the factors such as pH, salt and temperature on the physical properties of charged nanomaterials. Lastly, we have summarized the excellent engineering of various pH-induced charge reversible nanomaterials in imaging and therapy. These nanomaterials have acid-labile bonds or ionizable groups which endow

View Article Online
DOI: 10.1039/D4NR03706E

them with pH-responsiveness. The ability to freely change a material's structure during its fabrication stage allows us to finely control its charges at specific pH *in vivo* which is a gift for precise targeted delivery. By controlling the charges on the nanomaterial, we are better able to predict their physicochemical properties in the body such as their colloidal stability and size and ultimately, their fate *in vivo*. This ability to tap on the magic of pH and charges have introduced us to pH-induced charge switchable systems where materials with ionizable groups become protonated or deprotonated depending on their surrounding pH levels. This is especially useful for the delicate balance of prolonged circulation time and efficient cellular uptake: a negatively charged or neutral nanomaterial has a longer circulation time, but it can become positively charged in an acidic environment which will facilitate its penetration through the cell membrane. Many nanotheranostic systems have leveraged this pH-triggered charge switch to enter certain cells and amplify signals for imaging and target delivery of therapeutics. Coupled with the advancement in imaging capabilities in recent years, nanotheranostic is more promising now than ever.

However, there are some challenges that pH-responsive theranostic face. The complexity and fluctuating nature of biological systems presents one of the greatest obstacles in translating these promising materials to the clinics. In some cases, the pH difference between normal and pathological tissues are too small (approximately 0.3 – 0.7) to induce a pH-triggered release (*152*). Moreover, the pH within tumours is heterogeneous which can be difficult to design chemical compounds to target those cancerous tissues precisely. The narrow pH window for pH-induced bond cleavage or ionization adds another complexity in designing these charge switchable nanoparticles. In addition, many of the reported nanomaterials, especially the inorganic ones, are non-biodegradable. Hence, there should be more efforts directed to study and improve the biodegradation of these materials *in vivo*. If the non-biodegradable starting materials cannot be replaced with biodegradable ones, there should be more attention paid to their long-term toxicity *in vivo* to ensure their safety in clinical applications. Furthermore, these nanomaterials should preferably be prepared in a facile and green manner.

A critical consideration for *in vivo* applications is to minimize the undesirable non-specific binding of biomolecules on nanomaterials' surfaces as this can severely compromise their performance. Fortunately, zwitterionic materials have proven to be more effective and safe compared to traditional non-fouling PEGylated materials (*78*). As we aim for nanomaterials to have a long circulation time in the body (large particle size), we also value rapid clearance of the nanomaterials after performing their theranostic activities (small particle size). Therein lies the size dilemma between efficient clearance from the body and reduction in residence time for accumulation in target tissues (*54*). Like how pH-induced charge reversal nanosystems can address the polycation dilemma, pH-dependent size changes can overcome this dilemma. For instance, small nanoparticles can aggregate in the presence of an acidic tumor microenvironment to allow for efficient accumulation in the tumor tissues while the small untargeted nanoparticles can be removed quickly via renal clearance.

In addition, a significantly large proportion of pH-induced charge switchable theranostic nanomaterials reported in recent years (2020 – 2024) are for cancer. This skewed statistic is reasonable as the global burden for cancer is very high. However, we feel that pH as an endogenous stimulus to trigger a charge switch is highly unique and should be investigated for other diseases that have a different pH from healthy tissues. Besides cancer and bacterial infection, the distinct pH variation along the gastrointestinal tract can also be explored for pH-induced charge reversal nanosystems. The alkaline pH of the colon has been targeted for pH-triggered negative to positive charge conversion for promoting the adhesion and accumulation of nanocarriers in the inflamed colonic tissues of ulcerative colitis mice (*153, 154*). However, both studies did not go further than *ex vivo* fluorescence imaging. Since fluorescence probes are already present in their nanomaterial, incorporating real time *in vivo*

View Article Online
DOI: 10.1039/D4NR03706E

fluorescence imaging would have value added to their nanomaterials for theranostic applications. There is so much potential for tapping into pH-triggered charge reversal for theranostic purposes in other diseases due to the unique advantages offered by the distinct pH environments and charge switching *in vivo*. We look forward to the exciting developments with nanomaterials targeted at diseases aside from cancer and bacterial infection.

In conclusion, pH and charges are very much interconnected. Changing pH can tailor the surface charges of a nanomaterial. Similarly, incorporating a weak electrolyte as a charged component in a mixed-charge material can endow the nanomaterial with pH-sensitivity. This review provides a useful guideline for designing pH-responsive nanomaterials capable of charge conversion for theranostic purposes. We believe that theranostic has so much potential in clinical settings as it combines both diagnostic and therapeutic modalities into one system. This two-in-one approach can reduce the administration of the nanomaterial into the body and may reduce healthcare costs. Certainly, smart nanotheranostic with pH-triggered charge switch offers new possibilities for their clinical applications in theranostic.

References

1. J. Funkhouser, Reintroducing pharma: Theranostic revolution. *Current Drug Discovery*, (2002).
2. S. S. Kelkar, T. M. Reineke, Theranostics: Combining Imaging and Therapy. *Bioconjugate Chemistry* **22**, 1879-1903 (2011).
3. P. Das, M. K. Das, in *Multifunctional Theranostic Nanomedicines in Cancer,* M. K. Das, Ed. (Academic Press, 2021), pp. 1-24.
4. Y. Huang, S. He, W. Cao, K. Cai, X.-J. Liang, Biomedical nanomaterials for imaging-guided cancer therapy. *Nanoscale* **4**, 6135-6149 (2012).
5. O. Koshkina *et al.*, Biodegradable polyphosphoester micelles act as both background-free 31P magnetic resonance imaging agents and drug nanocarriers. *Nature Communications* **14**, 4351 (2023).
6. H. Zhou *et al.*, Theranostic imaging and multimodal photodynamic therapy and immunotherapy using the mTOR signaling pathway. *Nature Communications* **14**, 5350 (2023).
7. J. Li *et al.*, Boron encapsulated in a liposome can be used for combinational neutron capture therapy. *Nature Communications* **13**, 2143 (2022).
8. Q. Chen *et al.*, Target Functionalized Carbon Dot Nanozymes with Dual-Model Photoacoustic and Fluorescence Imaging for Visual Therapy in Atherosclerosis. *Advanced Science* **11**, 2307441 (2024).
9. B. Ma *et al.*, Reactive Oxygen Species Responsive Theranostic Nanoplatform for Two-Photon Aggregation-Induced Emission Imaging and Therapy of Acute and Chronic Inflammation. *ACS Nano* **14**, 5862-5873 (2020).
10. K. X. Vazquez-Prada *et al.*, A Spiky Silver-Iron Oxide Nanoparticle for Highly Efficient Targeted Photothermal Therapy and Multimodal Imaging of Thrombosis. *Small* **19**, 2205744 (2023).
11. M. T. Au *et al.*, Nerve Growth Factor-Targeted Molecular Theranostics Based on Molybdenum Disulfide Nanosheet-Coated Gold Nanorods (MoS2-AuNR) for Osteoarthritis Pain. *ACS Nano* **15**, 11711-11723 (2021).
12. X. Chen *et al.*, An MMP-2 Responsive Nanotheranostic Probe Enabled Synergistic Therapy of Rheumatoid Arthritis and MR/CT Assessment of Therapeutic Response In Situ. *Advanced Healthcare Materials* **12**, 2300962 (2023).
13. J. Chen *et al.*, Tocilizumab–Conjugated Polymer Nanoparticles for NIR-II Photoacoustic-Imaging-Guided Therapy of Rheumatoid Arthritis. *Advanced Materials* **32**, 2003399 (2020).
14. D.-Y. Zhang *et al.*, Biodegradable Self-Assembled Ultrasmall Nanodots as Reactive Oxygen/Nitrogen Species Scavengers for Theranostic Application in Acute Kidney Injury. *Small* **17**, 2005113 (2021).
15. K. Zhang *et al.*, Renal Endothelial Cell-Targeted Extracellular Vesicles Protect the Kidney from Ischemic Injury. *Advanced Science* **10**, 2204626 (2023).
16. D.-Y. Zhang *et al.*, Ultrasmall platinum nanozymes as broad-spectrum antioxidants for theranostic application in acute kidney injury. *Chemical Engineering Journal* **409**, 127371 (2021).
17. C. Wang *et al.*, Amyloid-β Oligomer-Targeted Gadolinium-Based NIR/MR Dual-Modal Theranostic Nanoprobe for Alzheimer's Disease. *Advanced Functional Materials* **30**, 1909529 (2020).

18. C. He *et al.*, Multifunctional bioreactive-nanoconstructs for sensitive and accurate MRI of cerebrospinal fluid pathology and intervention of Alzheimer's disease. *Nano Today* **35**, 100965 (2020).
19. T. Zhang *et al.*, Near-Infrared Aggregation-Induced Emission Luminogens for In Vivo Theranostics of Alzheimer's Disease. *Angewandte Chemie International Edition* **62**, e202211550 (2023).
20. Y. Zhou, W. Wu, P. Yang, D. Mao, B. Liu, Near-infrared chemiluminescent nanoprobes for deep imaging and synergistic photothermal-nitric-oxide therapy of bacterial infection. *Biomaterials* **288**, 121693 (2022).
21. Z. Mei *et al.*, Activatable NIR-II photoacoustic imaging and photochemical synergistic therapy of MRSA infections using miniature Au/Ag nanorods. *Biomaterials* **251**, 120092 (2020).
22. M. Wu *et al.*, HClO-Activated Fluorescence and Photosensitization from an AIE Nanoprobe for Image-Guided Bacterial Ablation in Phagocytes. *Advanced Materials* **32**, 2005222 (2020).
23. R. Vinhas *et al.*, Gold nanoparticle-based theranostics: disease diagnostics and treatment using a single nanomaterial. *Nanobiosensors in Disease Diagnosis* **4**, 11-23 (2015).
24. L.-S. Wang, M.-C. Chuang, J.-a. A. Ho, Nanotheranostics – a review of recent publications. *International Journal of Nanomedicine* **7**, 4679-4695 (2012).
25. J. Nam *et al.*, Cancer nanomedicine for combination cancer immunotherapy. *Nature Reviews Materials* **4**, 398-414 (2019).
26. H. Maeda, J. Wu, T. Sawa, Y. Matsumura, K. Hori, Tumor vascular permeability and the EPR effect in macromolecular therapeutics: a review. *Journal of Controlled Release* **65**, 271-284 (2000).
27. X. Han *et al.*, The Applications of Magnetic Particle Imaging: From Cell to Body. *Diagnostics (Basel)* **10**, (2020).
28. Z. Cheng *et al.*, Application of serum SERS technology based on thermally annealed silver nanoparticle composite substrate in breast cancer. *Photodiagnosis and Photodynamic Therapy* **41**, 103284 (2023).
29. P. Mi, Stimuli-responsive nanocarriers for drug delivery, tumor imaging, therapy and theranostics. *Theranostics* **10**, 4557-4588 (2020).
30. D. Wei, Y. Sun, H. Zhu, Q. Fu, Stimuli-Responsive Polymer-Based Nanosystems for Cancer Theranostics. *ACS Nano* **17**, 23223-23261 (2023).
31. M. Zeng *et al.*, The Integration of Nanomedicine with Traditional Chinese Medicine: Drug Delivery of Natural Products and Other Opportunities. *Mol Pharm* **20**, 886-904 (2023).
32. L. Palanikumar *et al.*, pH-Responsive Upconversion Mesoporous Silica Nanospheres for Combined Multimodal Diagnostic Imaging and Targeted Photodynamic and Photothermal Cancer Therapy. *ACS Nano* **17**, 18979-18999 (2023).
33. F. Veider, E. Sanchez Armengol, A. Bernkop-Schnürch, Charge-Reversible Nanoparticles: Advanced Delivery Systems for Therapy and Diagnosis. *Small* **20**, 2304713 (2024).
34. H. Y. Yang, Y. Li, D. S. Lee, Recent Advances of pH-Induced Charge-Convertible Polymer-Mediated Inorganic Nanoparticles for Biomedical Applications. *Macromolecular Rapid Communications* **41**, 2000106 (2020).
35. Z. Zhang, L. Wang, Z. Guo, Y. Sun, J. Yan, A pH-sensitive imidazole grafted polymeric micelles nanoplatform based on ROS amplification for ferroptosis-

enhanced chemodynamic therapy. *Colloids Surf B Biointerfaces* **237**, 113871 (2024).
36. H. Li, X. Li, J. Ji, Mixed-charge bionanointerfaces: Opposite charges work in harmony to meet the challenges in biomedical applications. *WIREs Nanomedicine and Nanobiotechnology* **12**, e1600 (2020).
37. J. Choi, M. F. Rubner, Influence of the Degree of Ionization on Weak Polyelectrolyte Multilayer Assembly. *Macromolecules* **38**, 116-124 (2005).
38. Z. Y. Zhu, S. Karlin, Clusters of charged residues in protein three-dimensional structures. *Proceedings of the National Academy of Sciences* **93**, 8350-8355 (1996).
39. J. Lipfert, S. Doniach, R. Das, D. Herschlag, Understanding Nucleic Acid–Ion Interactions. *Annual Review of Biochemistry* **83**, 813-841 (2014).
40. S. McLaughlin, The Electrostatic Properties of Membranes. *Annual Review of Biophysics and Biophysical Chemistry* **18**, 113-136 (1989).
41. Y. Ma, K. Poole, J. Goyette, K. Gaus, Introducing Membrane Charge and Membrane Potential to T Cell Signaling. *Frontiers in Immunology* **8**, (2017).
42. L. Li, X. Shi, X. Guo, H. Li, C. Xu, Ionic protein–lipid interaction at the plasma membrane: what can the charge do? *Trends in Biochemical Sciences* **39**, 130-140 (2014).
43. T. J. Silhavy, D. Kahne, S. Walker, The Bacterial Cell Envelope. *Cold Spring Harbor Perspectives in Biology* **2**, (2010).
44. Y. Shai, Mode of action of membrane active antimicrobial peptides. *Peptide Science* **66**, 236-248 (2002).
45. F. Alexis, E. Pridgen, L. K. Molnar, O. C. Farokhzad, Factors Affecting the Clearance and Biodistribution of Polymeric Nanoparticles. *Molecular Pharmaceutics* **5**, 505-515 (2008).
46. E. Fröhlich, The role of surface charge in cellular uptake and cytotoxicity of medical nanoparticles. *International Journal of Nanomedicine* **7**, 5577-5591 (2012).
47. A. Verma, F. Stellacci, Effect of Surface Properties on Nanoparticle–Cell Interactions. *Small* **6**, 12-21 (2010).
48. A. Albanese, P. S. Tang, W. C. W. Chan, The Effect of Nanoparticle Size, Shape, and Surface Chemistry on Biological Systems. *Annual Review of Biomedical Engineering* **14**, 1-16 (2012).
49. E. C. Cho, J. Xie, P. A. Wurm, Y. Xia, Understanding the Role of Surface Charges in Cellular Adsorption versus Internalization by Selectively Removing Gold Nanoparticles on the Cell Surface with a I2/KI Etchant. *Nano Letters* **9**, 1080-1084 (2009).
50. J. Wu, The Enhanced Permeability and Retention (EPR) Effect: The Significance of the Concept and Methods to Enhance Its Application. *J Pers Med* **11**, (2021).
51. J. Liu *et al.*, Redox/pH-responsive hollow manganese dioxide nanoparticles for thyroid cancer treatment. *Frontiers in Chemistry* **11**, (2023).
52. G.-R. Tan, C.-Y. S. Hsu, Y. Zhang, pH-Responsive Hybrid Nanoparticles for Imaging Spatiotemporal pH Changes in Biofilm-Dentin Microenvironments. *ACS Applied Materials & Interfaces* **13**, 46247-46259 (2021).
53. B. D. Ratner, A. S. Hoffman, in *Biomaterials Science (Third Edition),* B. D. Ratner, A. S. Hoffman, F. J. Schoen, J. E. Lemons, Eds. (Academic Press, 2013), pp. 241-247.

54. J. Nam *et al.*, Surface engineering of inorganic nanoparticles for imaging and therapy. *Advanced Drug Delivery Reviews* **65**, 622-648 (2013).
55. D. E. Owens, N. A. Peppas, Opsonization, biodistribution, and pharmacokinetics of polymeric nanoparticles. *International Journal of Pharmaceutics* **307**, 93-102 (2006).
56. X.-Q. Zhang *et al.*, Interactions of nanomaterials and biological systems: Implications to personalized nanomedicine. *Advanced Drug Delivery Reviews* **64**, 1363-1384 (2012).
57. X. Li, Y. Huang, Q. Jin, J. Ji, Mixed-charge modification as a robust method to realize the antiviral ability of gold nanoparticles in a high protein environment. *Nanoscale* **13**, 19857-19863 (2021).
58. S. Chen, L. Li, C. Zhao, J. Zheng, Surface hydration: Principles and applications toward low-fouling/nonfouling biomaterials. *Polymer* **51**, 5283-5293 (2010).
59. S. H. Lim, T. W. Wong, W. X. Tay, Overcoming colloidal nanoparticle aggregation in biological milieu for cancer therapeutic delivery: Perspectives of materials and particle design. *Advances in Colloid and Interface Science* **325**, 103094 (2024).
60. L. Guerrini, R. A. Alvarez-Puebla, N. Pazos-Perez, Surface Modifications of Nanoparticles for Stability in Biological Fluids. *Materials* **11**, 1154 (2018).
61. T. L. Moore *et al.*, Nanoparticle colloidal stability in cell culture media and impact on cellular interactions. *Chemical Society Reviews* **44**, 6287-6305 (2015).
62. X. Liu, H. Huang, Q. Jin, J. Ji, Mixed Charged Zwitterionic Self-Assembled Monolayers as a Facile Way to Stabilize Large Gold Nanoparticles. *Langmuir* **27**, 5242-5251 (2011).
63. Y. Nie *et al.*, Metal organic framework coated MnO(2) nanosheets delivering doxorubicin and self-activated DNAzyme for chemo-gene combinatorial treatment of cancer. *Int J Pharm* **585**, 119513 (2020).
64. J. Liu *et al.*, pH-Sensitive nano-systems for drug delivery in cancer therapy. *Biotechnology Advances* **32**, 693-710 (2014).
65. N. M. AlSawaftah, N. S. Awad, W. G. Pitt, G. A. Husseini, pH-Responsive Nanocarriers in Cancer Therapy. *Polymers* **14**, 936 (2022).
66. S. Chu, X. Shi, Y. Tian, F. Gao, pH-Responsive Polymer Nanomaterials for Tumor Therapy. *Front Oncol* **12**, 855019 (2022).
67. L. Palanikumar *et al.*, pH-responsive high stability polymeric nanoparticles for targeted delivery of anticancer therapeutics. *Communications Biology* **3**, 95 (2020).
68. C. Zhang *et al.*, Stepwise pH-responsive nanoparticles containing charge-reversible pullulan-based shells and poly (β-amino ester)/poly (lactic-co-glycolic acid) cores as carriers of anticancer drugs for combination therapy on hepatocellular carcinoma. *Journal of controlled release* **226**, 193-204 (2016).
69. X. Qu, Z. Yang, Benzoic-imine-based physiological-pH-responsive materials for biomedical applications. *Chemistry–An Asian Journal* **11**, 2633-2641 (2016).
70. P. Zhang, D. Chen, L. Li, K. Sun, Charge reversal nano-systems for tumor therapy. *Journal of Nanobiotechnology* **20**, 31 (2022).
71. R. Y. H. Tan, C. S. Lee, M. R. Pichika, S. F. Cheng, K. Y. Lam, PH Responsive Polyurethane for the Advancement of Biomedical and Drug Delivery. *Polymers* **14**, 1672 (2022).

View Article Online
DOI:10.1039/D4NR03706E

72. N. Deirram, C. Zhang, S. S. Kermaniyan, A. P. Johnston, G. K. Such, pH-responsive polymer nanoparticles for drug delivery. *Macromolecular rapid communications* **40**, 1800917 (2019).
73. M. Li *et al.*, Fabrication of Charge-Conversion Nanoparticles for Cancer Imaging by Flash Nanoprecipitation. *ACS Applied Materials & Interfaces* **10**, 10752-10760 (2018).
74. R. U. Khan, J. Shao, J.-Y. Liao, L. Qian, pH-triggered cancer-targeting polymers: From extracellular accumulation to intracellular release. *Nano Research* **16**, 5155-5168 (2023).
75. N. Jia *et al.*, Tumor Microenvironment Stimuli-Responsive Nanoparticles for Programmed Anticancer Drug Delivery. *Molecular Pharmaceutics* **17**, 1516-1526 (2020).
76. S. Y. Fam *et al.*, Stealth Coating of Nanoparticles in Drug-Delivery Systems. *Nanomaterials* **10**, 787 (2020).
77. J. Cao, Y. W. Chen, X. Wang, X. L. Luo, Enhancing blood compatibility of biodegradable polymers by introducing sulfobetaine. *Journal of Biomedical Materials Research Part A* **97**, 472-479 (2011).
78. Q. Li *et al.*, Zwitterionic Biomaterials. *Chemical Reviews* **122**, 17073-17154 (2022).
79. Y. Wang *et al.*, Fabrication of zwitterionic and pH-responsive polyacetal dendrimers for anticancer drug delivery. *Biomaterials Science* **7**, 3238-3248 (2019).
80. E. Pramod Kumar, W. Um, J. H. Park, Recent developments in pathological pH-responsive polymeric nanobiosensors for cancer theranostics. *Front. Bioeng. Biotechnol.* **8**, 601586 (2020).
81. L. D. Blackman, P. A. Gunatillake, P. Cass, K. E. S. Locock, An introduction to zwitterionic polymer behavior and applications in solution and at surfaces. *Chemical Society Reviews* **48**, 757-770 (2019).
82. S. Bazban-Shotorbani *et al.*, Revisiting structure-property relationship of pH-responsive polymers for drug delivery applications. *J. Control. Release* **253**, 46-63 (2017).
83. W. Wu *et al.*, Endogenous pH-responsive nanoparticles with programmable size changes for targeted tumor therapy and imaging applications. *Theranostics* **8**, 3038 (2018).
84. X. Liu *et al.*, Enhanced Retention and Cellular Uptake of Nanoparticles in Tumors by Controlling Their Aggregation Behavior. *ACS Nano* **7**, 6244-6257 (2013).
85. M. Borkowska *et al.*, Targeted crystallization of mixed-charge nanoparticles in lysosomes induces selective death of cancer cells. *Nature Nanotechnology* **15**, 331-341 (2020).
86. A. B. Lowe, C. L. McCormick, Synthesis and Solution Properties of Zwitterionic Polymers. *Chemical Reviews* **102**, 4177-4190 (2002).
87. P. P. Pillai, S. Huda, B. Kowalczyk, B. A. Grzybowski, Controlled pH Stability and Adjustable Cellular Uptake of Mixed-Charge Nanoparticles. *Journal of the American Chemical Society* **135**, 6392-6395 (2013).
88. M. Siek, K. Kandere-Grzybowska, B. A. Grzybowski, Mixed-Charge, pH-Responsive Nanoparticles for Selective Interactions with Cells, Organelles, and Bacteria. *Accounts of Materials Research* **1**, 188-200 (2020).
89. S. E. Kudaibergenov, Advances in Synthetic Polyampholytes for Biotechnology and Medicine. *Review Journal of Chemistry* **10**, 12-39 (2020).

90. A. Erfani, J. Seaberg, C. P. Aichele, J. D. Ramsey, Interactions between biomolecules and zwitterionic moieties: a review. *Biomacromolecules* **21**, 2557-2573 (2020).
91. J. Ning, K. Kubota, G. Li, K. Haraguchi, Characteristics of zwitterionic sulfobetaine acrylamide polymer and the hydrogels prepared by free-radical polymerization and effects of physical and chemical crosslinks on the UCST. *React. Funct. Polym.* **73**, 969-978 (2013).
92. L. Chen *et al.*, Effects of polyelectrolyte complexation on the UCST of zwitterionic polymer. *Polymer* **41**, 141-147 (2000).
93. Q. Lin *et al.*, The Thermogel Chronicle—From Rational Design of Thermogelling Copolymers to Advanced Thermogel Applications. *Acc. Mater. Res.* **2**, 881-894 (2021).
94. E. Boedtkjer, S. F. Pedersen, The Acidic Tumor Microenvironment as a Driver of Cancer. *Annual Review of Physiology* **82**, 103-126 (2020).
95. R. Yamamura, K. Y. Inoue, K. Nishino, S. Yamasaki, Intestinal and fecal pH in human health. *Frontiers in Microbiomes* **2**, (2023).
96. M. Lee-Rueckert *et al.*, Acidic extracellular pH promotes accumulation of free cholesterol in human monocyte-derived macrophages via inhibition of ACAT1 activity. *Atherosclerosis* **312**, 1-7 (2020).
97. L. A. Schneider, A. Korber, S. Grabbe, J. Dissemond, Influence of pH on wound-healing: a new perspective for wound-therapy? *Archives of Dermatological Research* **298**, 413-420 (2007).
98. B. R. Smith, S. S. Gambhir, Nanomaterials for In Vivo Imaging. *Chemical Reviews* **117**, 901-986 (2017).
99. S. Yoon *et al.*, Recent advances in optical imaging through deep tissue: imaging probes and techniques. *Biomaterials Research* **26**, 57 (2022).
100. H. Qi *et al.*, Electrospun green fluorescent-highly anisotropic conductive Janus-type nanoribbon hydrogel array film for multiple stimulus response sensors. *Composites Part B: Engineering* **288**, 111933 (2025).
101. M. J. Sanderson, I. Smith, I. Parker, M. D. Bootman, Fluorescence microscopy. *Cold Spring Harb Protoc* **2014**, pdb top071795 (2014).
102. R. T. Sadikot, T. S. Blackwell, Bioluminescence imaging. *Proc Am Thorac Soc* **2**, 537-540, 511-532 (2005).
103. C. Chen *et al.*, Amplification of Activated Near-Infrared Afterglow Luminescence by Introducing Twisted Molecular Geometry for Understanding Neutrophil-Involved Diseases. *J Am Chem Soc* **144**, 3429-3441 (2022).
104. L. Li *et al.*, A pH-responsive magnetic resonance tuning probe for precise imaging of bacterial infection in vivo. *Acta Biomater* **164**, 487-495 (2023).
105. G.-C. Zhang *et al.*, Bismuth-Based Mesoporous Nanoball Carrying Sorafenib for Computed Tomography Imaging and Synergetic Chemoradiotherapy of Hepatocellular Carcinoma. *Advanced Healthcare Materials* **9**, 2000650 (2020).
106. J. Zhu *et al.*, 131I-Labeled Multifunctional Polyethylenimine/Doxorubicin Complexes with pH-Controlled Cellular Uptake Property for Enhanced SPECT Imaging and Chemo/Radiotherapy of Tumors. *International Journal of Nanomedicine* **16**, 5167-5183 (2021).
107. J. A.-T. Walker, X. Wang, K. Peter, K. Kempe, S. R. Corrie, Dynamic Solid-State Ultrasound Contrast Agent for Monitoring pH Fluctuations In Vivo. *ACS Sensors* **5**, 1190-1197 (2020).

View Article Online
DOI: 10.1039/D4NR03706E

108. Z. Yang *et al.*, A pH-responsive photoacoustic imaging probe for tumor pH imaging in vivo based on polyaniline-bovine serum albumin. *Nanomedicine* **33**, 102356 (2021).
109. Q. Ci *et al.*, Fe-Doped Carbon Dots as NIR-II Fluorescence Probe for In Vivo Gastric Imaging and pH Detection. *Adv Sci (Weinh)* **10**, e2206271 (2023).
110. X. Han, K. Xu, O. Taratula, K. Farsad, Applications of nanoparticles in biomedical imaging. *Nanoscale* **11**, 799-819 (2019).
111. Y. Cao, L. Xu, Y. Kuang, D. Xiong, R. Pei, Gadolinium-based nanoscale MRI contrast agents for tumor imaging. *Journal of Materials Chemistry B* **5**, 3431-3461 (2017).
112. Y. Chen *et al.*, Oxygen-Independent Radiodynamic Therapy: Radiation-Boosted Chemodynamics for Reprogramming the Tumor Immune Environment and Enhancing Antitumor Immune Response. *ACS Applied Materials & Interfaces* **16**, 21546-21556 (2024).
113. N. Lee, T. Hyeon, Designed synthesis of uniformly sized iron oxide nanoparticles for efficient magnetic resonance imaging contrast agents. *Chemical Society Reviews* **41**, 2575-2589 (2012).
114. X. Chen, Z. Jiang, X. Han, X. Wang, X. Tang, The Reconstruction of Magnetic Particle Imaging: Current Approaches Based on the System Matrix. *Diagnostics* **11**, 773 (2021).
115. H. Lu *et al.*, A pH-responsive T(1)-T(2) dual-modal MRI contrast agent for cancer imaging. *Nat Commun* **13**, 7948 (2022).
116. M. Shilo, T. Reuveni, M. Motiei, R. Popovtzer, Nanoparticles as computed tomography contrast agents: current status and future perspectives. *Nanomedicine* **7**, 257-269 (2012).
117. D. T. Ginat, R. Gupta, Advances in Computed Tomography Imaging Technology. *Annual Review of Biomedical Engineering* **16**, 431-453 (2014).
118. E. Lin, A. Alessio, What are the basic concepts of temporal, contrast, and spatial resolution in cardiac CT? *Journal of Cardiovascular Computed Tomography* **3**, 403-408 (2009).
119. J. Pellico, P. J. Gawne, R. T. M. de Rosales, Radiolabelling of nanomaterials for medical imaging and therapy. *Chemical Society Reviews* **50**, 3355-3423 (2021).
120. P. J. Gawne, F. Man, P. J. Blower, R. T. M. de Rosales, Direct Cell Radiolabeling for in Vivo Cell Tracking with PET and SPECT Imaging. *Chemical Reviews* **122**, 10266-10318 (2022).
121. Y. Ju, B. Dong, J. Yu, Y. Hou, Inherent multifunctional inorganic nanomaterials for imaging-guided cancer therapy. *Nano Today* **26**, 108-122 (2019).
122. X. Han *et al.*, Ultrasound-responsive smart composite biomaterials in tissue repair. *Nano Today* **49**, 101804 (2023).
123. B. Chu *et al.*, Fluorescence, ultrasonic and photoacoustic imaging for analysis and diagnosis of diseases. *Chemical Communications* **59**, 2399-2412 (2023).
124. F. Tian *et al.*, Acoustic-Based Theranostic Probes Activated by Tumor Microenvironment for Accurate Tumor Diagnosis and Assisted Tumor Therapy. *ACS Sensors* **7**, 3611-3633 (2022).
125. Q. Miao, K. Pu, Organic Semiconducting Agents for Deep-Tissue Molecular Imaging: Second Near-Infrared Fluorescence, Self-Luminescence, and Photoacoustics. *Advanced Materials* **30**, 1801778 (2018).

126. H. F. Zhang, K. Maslov, G. Stoica, L. V. Wang, Functional photoacoustic microscopy for high-resolution and noninvasive in vivo imaging. *Nat Biotechnol* **24**, 848-851 (2006).
127. J.-J. Li *et al.*, Lactose azocalixarene drug delivery system for the treatment of multidrug-resistant pseudomonas aeruginosa infected diabetic ulcer. *Nature Communications* **13**, 6279 (2022).
128. D. Hu, Y. Deng, F. Jia, Q. Jin, J. Ji, Surface Charge Switchable Supramolecular Nanocarriers for Nitric Oxide Synergistic Photodynamic Eradication of Biofilms. *ACS Nano* **14**, 347-359 (2020).
129. W. Li *et al.*, pH/Hyal-Responsive Surface-Charge Switchable Electrostatic Complexation for Efficient Elimination of MRSA Infection. *Molecular Pharmaceutics* **20**, 3683-3692 (2023).
130. T. Liu *et al.*, Surface charge switchable nanoparticles capable of controlled nitric oxide release for the treatment of acidity-associated bacterial infections. *Polymer Chemistry* **12**, 1023-1029 (2021).
131. L. Yang *et al.*, pH-Responsive Hyperbranched Polymer Nanoparticles to Combat Intracellular Infection by Disrupting Bacterial Wall and Regulating Macrophage Polarization. *Biomacromolecules* **23**, 4370-4378 (2022).
132. Z. Guo *et al.*, pH-Responsive charge switchable PEGylated ε-poly-l-lysine polymeric nanoparticles-assisted combination therapy for improving breast cancer treatment. *Journal of Controlled Release* **326**, 350-364 (2020).
133. X. Li *et al.*, Intelligent nanogels with self-adaptive responsiveness for improved tumor drug delivery and augmented chemotherapy. *Bioactive Materials* **6**, 3473-3484 (2021).
134. B. Zhou *et al.*, Engineering polyzwitterion with acylsulfonamide-based betaine structure for protonated switch of surface chemistry at tumoral pH and reductive responsive drug release of polymeric micelles. *Materials Today Chemistry* **17**, 100339 (2020).
135. R. Yang *et al.*, Charge and Size Dual Switchable Nanocage for Novel Triple-Interlocked Combination Therapy Pattern. *Advanced Science* **7**, 2000906 (2020).
136. K. Qian *et al.*, Cholinergic Neuron Targeting Nanosystem Delivering Hybrid Peptide for Combinatorial Mitochondrial Therapy in Alzheimer's Disease. *ACS Nano* **16**, 11455-11472 (2022).
137. M. Ding, W. Zhao, X. Zhang, L. Song, S. Luan, Charge-switchable MOF nanocomplex for enhanced biofilm penetration and eradication. *Journal of Hazardous Materials* **439**, 129594 (2022).
138. M. Overchuk, R. A. Weersink, B. C. Wilson, G. Zheng, Photodynamic and Photothermal Therapies: Synergy Opportunities for Nanomedicine. *ACS Nano* **17**, 7979-8003 (2023).
139. Z. Gong, Z. Dai, Design and Challenges of Sonodynamic Therapy System for Cancer Theranostics: From Equipment to Sensitizers. *Advanced Science* **8**, 2002178 (2021).
140. J. Zeng *et al.*, Combined photothermal and sonodynamic therapy using a 2D black phosphorus nanosheets loaded coating for efficient bacterial inhibition and bone-implant integration. *Biomaterials* **297**, 122122 (2023).
141. X. Hu *et al.*, Emerging photodynamic/sonodynamic therapies for urological cancers: progress and challenges. *Journal of Nanobiotechnology* **20**, 437 (2022).

142. H. Ma *et al.*, Surface charge adaptive nitric oxide nanogenerator for enhanced photothermal eradication of drug-resistant biofilm infections. *Bioactive Materials* **27**, 154-167 (2023).
143. J. Kong *et al.*, Photothermal and Photocatalytic Glycol Chitosan and Polydopamine-Grafted Oxygen Vacancy Bismuth Oxyiodide (BiO1-xI) Nanoparticles for the Diagnosis and Targeted Therapy of Diabetic Wounds. *Advanced Materials* **36**, 2307695 (2024).
144. L.-X. Yan, L.-J. Chen, X. Zhao, X.-P. Yan, pH Switchable Nanoplatform for In Vivo Persistent Luminescence Imaging and Precise Photothermal Therapy of Bacterial Infection. *Advanced Functional Materials* **30**, 1909042 (2020).
145. Q. Wang *et al.*, Fluoropolymer-MOF Hybrids with Switchable Hydrophilicity for 19F MRI-Monitored Cancer Therapy. *ACS Nano* **17**, 8483-8498 (2023).
146. J. Zhu *et al.*, Surface-Charge-Switchable Nanoclusters for Magnetic Resonance Imaging-Guided and Glutathione Depletion-Enhanced Photodynamic Therapy. *ACS Nano* **14**, 11225-11237 (2020).
147. X. Shi *et al.*, Unimolecule-based size-charge switchable nanomedicine for deep cancer sono-immunotherapy. *Nano Today* **43**, 101417 (2022).
148. K. Zhu *et al.*, pH-Activatable Organic Nanoparticles for Efficient Low-Temperature Photothermal Therapy of Ocular Bacterial Infection. *ACS Nano* **16**, 11136-11151 (2022).
149. Z. Li *et al.*, Charge-reversal nanomedicine based on black phosphorus for the development of A Novel photothermal therapy of oral cancer. *Drug Delivery* **28**, 700-708 (2021).
150. N. Peng *et al.*, Sequential-targeting nanocarriers with pH-controlled charge reversal for enhanced mitochondria-located photodynamic-immunotherapy of cancer. *Acta Biomaterialia* **105**, 223-238 (2020).
151. J. Zhu *et al.*, Charge-conversional polyethylenimine-entrapped gold nanoparticles with 131I-labeling for enhanced dual mode SPECT/CT imaging and radiotherapy of tumors. *Biomaterials Science* **8**, 3956-3965 (2020).
152. R. A. Verkhovskii *et al.*, Current Principles, Challenges, and New Metrics in pH-Responsive Drug Delivery Systems for Systemic Cancer Therapy. *Pharmaceutics* **15**, 1566 (2023).
153. M. A. Oshi *et al.*, Curcumin Nanocrystal/pH-Responsive Polyelectrolyte Multilayer Core–Shell Nanoparticles for Inflammation-Targeted Alleviation of Ulcerative Colitis. *Biomacromolecules* **21**, 3571-3581 (2020).
154. N. Wang *et al.*, 5-aminosalicylic acid pH sensitive core-shell nanoparticles targeting ulcerative colitis. *Journal of Drug Delivery Science and Technology* **74**, 103578 (2022).

View Article Online
DOI: 10.1039/D4NR03706E

Data Availability Statement

No primary research results, software or code have been included and no new data were generated or analysed as part of this review.